Electron gas beyond the random-phase approximation: Algebraic screening

F. Cornu*
Laboratoire de Physique Théorique et Hautes Energies, Université de Paris–Sud, Bâtiment 211, F-91405 Orsay, France

Ph. A. Martin
Institut de Physique Théorique, Ecole Polytechnique Fédérale de Lausanne, PHB-Ecublens, CH-1015 Lausanne, Switzerland
(Received 25 April 1991)

Using the standard many-body perturbation theory at finite temperature, we exhibit diagrams, not included in the usual random-phase-approximation ring summation, that lead to a $1/|\mathbf{x}|^{10}$ decay of the charge-charge correlation. The quantum origin of this absence of exponential screening is clearly displayed in a semiclassical representation of the electron gas by functional integration, where the effective potential obtained by chain summation is of the dipolar type.

PACS number(s): 05.30.Fk, 71.45.Gm

I. INTRODUCTION

In a recent paper [1], it has been shown that the quantum corrections to the classical equilibrium correlations of a Coulomb fluid decay algebraically fast for all values of the thermodynamical parameters. At high temperature, this is in sharp contrast with the exponential falloff of the classical Coulombic correlations that has been rigorously established in Refs. [2] and [3]. In particular, consider the simplest model for an electron gas, the one-component plasma; it is a system of identical point particles embedded in a continuous uniform rigid background of the opposite charge that ensures overall neutrality. If one expands the static density-density correlation function $S(\mathbf{x})$ of the quantum one-component plasma in powers of the Planck constant,

$$S(\mathbf{x})=S^{\mathrm{cl}}(\mathbf{x})+\hbar^2 S^{(2)}(\mathbf{x})+\hbar^4 S^{(4)}(\mathbf{x})+\cdots \quad (1.1)$$

one finds that, at the order $\hbar^4$,

$$\lim_{|\mathbf{x}|\to\infty} S^{(4)}(\mathbf{x})\approx \frac{7}{16\pi^2}\left[\frac{\beta}{m}\right]^2 \frac{1}{|\mathbf{x}|^{10}}, \quad (1.2)$$

where m is the mass of the electron and β is the inverse temperature. The behavior (1.2) is equivalent with the fact that the Fourier transform $S(\mathbf{k})$ of $S(\mathbf{x})$ is not analytic at $\mathbf{k}=\mathbf{0}$ (it must have a $|\mathbf{k}|^7$ term in in its small-$\mathbf{k}$ expansion). The result (1.2) has been obtained by means of the Wigner-Kirkwood expansion in a semiclassical regime where the effects the Fermi statistics have been neglected.

In the present work, we address the same problem from the viewpoint of the standard many-body perturbation theory at nonzero temperature, including now the effects of the Fermi statistics. It is well known that the usual random-phase approximation (RPA) leads to an effective potential whose zero-frequency component is of the Debye-Hückel form, and therefore decreases in space faster than any inverse power of the distance (see Sec. III A). The same is true for the structure function calculated in this approximation, $S_{\mathrm{RPA}}(\mathbf{x})$. Thus the RPA theory fails to predict the algebraic decay of the correlations. The purpose of this paper is to study in some details the simplest diagram, not included in the RPA ring summation, which gives rise to a nonexponential decay.

We proceed as follows. In Sec. II we first relate the effective potential and the structure factor to the proper polarization according to the usual diagrammatic rules. Moreover, in the small-$\mathbf{k}$ expansion of these quantities we take into account the constraints imposed by the known exact sum rules (second moment and compressibility sum rules). Thus the problem is reduced to the investigation of the small-$\mathbf{k}$ behavior of the proper polarization.

In Sec. III A we briefly recall the form of the proper polarization which leads to the RPA effective potential. Then, in Sec. III B, we consider the "prototype" graphs in which the bare Coulomb interaction lines are replaced by RPA interaction lines. The simplest prototype graph that contributes to the proper polarization beyond RPA involves the square of the RPA effective potential (see Fig. 3). This graph leads to an $1/|\mathbf{x}|^6$ decay of the zero-frequency component of the full effective potential and to a $1/|\mathbf{x}|^{10}$ ($1/|\mathbf{x}|^8$) decay of the structure function (the inverse static dielectric function). Moreover we argue that in the class of the ladder diagrams with N RPA interaction lines ($N\geq 2$), the above-mentioned graphs (corresponding to $N=2$) gives rise to the slowest possible decay. We therefore make the plausible conjecture that these types of decay hold generally in the quantum electron gas.

In Sec. IV, we show how one can recover the semiclassical result (1.2) by means of the Mayer diagrammatic expansion. For this we neglect again the Fermi statistics and use the functional integral representation of the electron gas. In this representation the quantum system of point electrons can be treated as an equivalent classical gas of charged random filaments (Brownian bridges). Here the random shape of the filaments, which originates from the intrinsic quantum fluctuations, plays the role of an internal degree of freedom. Thus we can apply the usual approximation scheme developed for the statistical mechanics of classical charged systems. In particular,

the analogue of the Debye-Hückel approximation (the chain summation) gives in this formalism a chain potential that can easily be related to the usual RPA effective potential without Fermi statistics (see Appendix C). For fixed filaments, this potential is of dipolar type: the picture is that two filaments with arbitrary shapes have a residual dipole-dipole interaction decreasing as $1/|\mathbf{x}|^3$. After averaging the shapes of the filaments, the chain potential decreases exponentially, and again, the slowest possible decay comes from the prototype graph involving the square of this chain potential (Sec. IV A). If one retains only the $\hbar^4$ contributions to any graph (Sec. IV B), the series can be exactly summed to produce the result (1.2). Then we see how the classical Stillinger-Lovett sum rule changes the $1/|\mathbf{x}|^6$ decay of the squared chain potential into an $1/|\mathbf{x}|^{10}$ behavior for the charge-charge correlation function.

II. GENERAL FORMALISM

In this section, we analyze the general form of the static density correlation function of the homogeneous electron gas

$$S(\mathbf{x})=\langle[\hat{n}(\mathbf{x})-\langle\hat{n}(\mathbf{x})\rangle][\hat{n}(\mathbf{0})-\langle\hat{n}(\mathbf{0})\rangle]\rangle\ , \tag{2.1}$$

where $\langle\hat{n}(\mathbf{x})\rangle$ denotes the grand canonical average of the density operator $\hat{n}(\mathbf{x})$ at the inverse temperature β and chemical potential μ.

We briefly recall the perturbative structure of $S(\mathbf{x})$ following the definitions of Ref. [4] (Sec. 32, p. 300). The imaginary time evolved density is

$$\hat{n}(\mathbf{x},\tau)=e^{(\hat{H}-\mu\hat{N})\tau/\hbar}\hat{n}(\mathbf{x})e^{-(\hat{H}-\mu\hat{N})\tau/\hbar}\ , \tag{2.2}$$

where $\hat{H}$ is the Hamiltonian and $\hat{N}$ is the particle number operator in the Fock space. Then the basic quantity to be considered is the ordered temperature function,

$$S(\mathbf{x},\tau)=\langle T\{[\hat{n}(\mathbf{x},\tau)-\langle\hat{n}(\mathbf{x},\tau)\rangle]\times[\hat{n}(\mathbf{0},0)-\langle\hat{n}(\mathbf{0},0)\rangle]\}\rangle\ . \tag{2.3}$$

The imaginary time correlation (2.3) is related to the static susceptibility $\chi(\mathbf{k})$ and dielectric function $\epsilon(\mathbf{k})$ by

$$\chi(\mathbf{k})=\epsilon^{-1}(\mathbf{k})-1=\frac{4\pi e^2}{|\mathbf{k}|^2}\frac{1}{\hbar}\int_0^{\beta\hbar}d\tau S(\mathbf{k},\tau)\ , \tag{2.4}$$

where e is the charge of the electron and $S(\mathbf{k},\tau)$ is the spatial Fourier transform of (2.3),

$$S(\mathbf{k},\tau)\equiv\int d\mathbf{x}\,e^{i\mathbf{k}\cdot\mathbf{x}}S(\mathbf{x},\tau)\ . \tag{2.5}$$

Relation (2.4) expresses the linear response of the electron gas to a static external charge. The basic link with perturbation theory is given by

$$S(\mathbf{x},\tau)=-\Pi(\mathbf{x},\tau)\ , \tag{2.6}$$

where $\Pi(\mathbf{x},\tau)$, the total polarization, consists of all the connected diagram in which the points $(\mathbf{x},\tau)$ and $(\mathbf{0},0)$ are joined by internal lines. [Relation (2.6) differs from Eq. (32.20) of Ref. [4] by a factor $\hbar$ which is included here in the definition of $\Pi(\mathbf{x},\tau)$.]

All the τ-dependent functions $f(\tau)$ in the finite-temperature perturbation formalism are periodic with a period of $2\beta\hbar$. We define the τ-Fourier transform by

$$f(\omega)\equiv\frac{1}{2\beta\hbar}\int_{-\beta\hbar}^{\beta\hbar}d\tau\,e^{i\omega\tau}f(\tau)=\frac{1}{2}\int_{-1}^{1}ds\,e^{i\omega\beta\hbar s}f(s)\ , \tag{2.7}$$

where, in the second equality of (2.7), f is written in terms of the dimensionless variable $s=\tau/\beta\hbar$. [Our definition (2.7) differs from that of Ref. [4] by a factor of $\beta\hbar$.] When the spatial Fourier transform is introduced as in (2.5), the coefficients of the polarization in Fourier representation are given by

$$\Pi(\mathbf{k},n)\equiv\Pi(\mathbf{k},\omega_{2n})=\tfrac{1}{2}\int_{-1}^{1}ds\,e^{2i\pi ns}\Pi(\mathbf{k},s)=\int_0^1 ds\,e^{2i\pi ns}\Pi(\mathbf{k},s)\ ,\quad n=0,\pm1,\pm2,\ldots \tag{2.8}$$

with $\omega_n=\pi n/\beta\hbar$. Only the frequencies ω_{2n} indexed by even integers occur because, according to (2.3) and (2.6), $\Pi(\mathbf{k},\tau)$ is periodic with a period $\beta\hbar$. Hence it follows from (2.6) and from the definitions (2.1), (2.2), and (2.3) that

$$S(\mathbf{k})=S(\mathbf{k},\tau=0)=-\sum_{n=-\infty}^{\infty}\Pi(\mathbf{k},n) \tag{2.9}$$

and from (2.4) that

$$\chi(\mathbf{k})=\epsilon^{-1}(\mathbf{k})-1=\frac{4\pi\beta e^2}{|\mathbf{k}|^2}\Pi(\mathbf{k},n=0)\ . \tag{2.10}$$

It is convenient to introduce the proper polarization $\Pi^*(\mathbf{x},\tau)$, i.e., the set of all polarization parts which cannot be separated into two polarization parts by cutting a single interaction line. The total polarization and the total proper polarization are linked by a Dyson equation which takes a simple algebraic form in the Fourier representation

$$\Pi(\mathbf{k},n)=\frac{\Pi^*(\mathbf{k},n)}{1-U_0(\mathbf{k})\Pi^*(\mathbf{k},n)} \tag{2.11}$$

with

$$U_0(\mathbf{k})=\frac{4\pi\beta e^2}{|\mathbf{k}|^2}\ . \tag{2.12}$$

The relation (2.11) can be put in an equivalent form in terms of the effective potential $U^{\text{eff}}(\mathbf{k},n)$

$$\Pi(\mathbf{k},n)=\Pi^*(\mathbf{k},n)+\Pi^*(\mathbf{k},n)U^{\text{eff}}(\mathbf{k},n)\Pi^*(\mathbf{k},n) \tag{2.13}$$

with

$$U^{\text{eff}}(\mathbf{k},n)=\frac{U_0(\mathbf{k})}{1-U_0(\mathbf{k})\Pi^*(\mathbf{k},n)}\ . \tag{2.14}$$

In the sequel, we shall use the known exact sum rules obeyed by $S(\mathbf{k})$ to constrain the form of the small-$\mathbf{k}$ expansion of $\Pi(\mathbf{k},n)$. It is indeed known that $S(\mathbf{k})$ satisfies

the following long-wavelength screening sum rule [5,6]:

$$\lim_{|\mathbf{k}|\to 0} S(\mathbf{k}) \approx \frac{1}{U_0(\mathbf{k})} \frac{\beta\hbar\omega_p}{2} \coth\left[\frac{\beta\hbar\omega_p}{2}\right] . \tag{2.15}$$

where $\omega_p \equiv (4\pi\rho e^2/m)^{1/2}$ is the plasma frequency, ρ is the number density, and m the mass of the electron. Moreover, the compressibility sum rules states that [5]

$$\lim_{|\mathbf{k}|\to 0} \epsilon(\mathbf{k}) \approx 1 + \frac{4\pi e^2 \rho \chi_T}{|\mathbf{k}|^2} , \tag{2.16}$$

where χ_T is the isothermal compressibility. Using the series representation of coth, we may write relation (2.15) as

$$\lim_{|\mathbf{k}|\to 0} S(\mathbf{k}) \approx \frac{|\mathbf{k}|^2}{4\pi\beta e^2} \sum_{n=-\infty}^{\infty} \frac{1}{1+4\pi^2 n^2/(\lambda\kappa_D)^2} , \tag{2.17}$$

where $\lambda = \hbar\sqrt{\beta/m}$ is the de Broglie thermal wavelength (up to a factor $\sqrt{2\pi}$) and $\kappa_D \equiv (4\pi\beta\rho e^2)^{1/2}$ is the inverse Debye length. Thus, since $\Pi(-\mathbf{k},-n) = \Pi(\mathbf{k},n)$, we see from (2.9) that

$$\lim_{|\mathbf{k}|\to 0} \Pi(\mathbf{k},n) \approx -\frac{1}{4\pi\beta e^2} \frac{1}{1+4\pi^2 n^2/(\lambda\kappa_D)^2} |\mathbf{k}|^2 . \tag{2.18}$$

Moreover, according to (2.10) the compressibility sum rule (2.16) determines the zero-frequency component $\Pi(\mathbf{k},n=0)$ up to the order $|\mathbf{k}|^4$,

$$\lim_{|\mathbf{k}|\to 0} \Pi(\mathbf{k},n=0) \approx -\frac{1}{4\pi\beta e^2} \left[|\mathbf{k}|^2 - \frac{|\mathbf{k}|^4}{4\pi e^2 \rho \chi_T} \right] . \tag{2.19}$$

We now exhibit how these constraints on $\Pi(\mathbf{k},n)$ restrain the expansion of $\Pi^*(\mathbf{k},n)$ in powers of $\mathbf{k}$. At this level, we assume that both $\Pi^*(\mathbf{k},n)$ and $\Pi(\mathbf{k},n)$ have small $\mathbf{k}$ expansions, up to $|\mathbf{k}|^7$, of the following form (because of rotational invariance, these quantities depend only on $|\mathbf{k}|$):

$$\Pi^*(\mathbf{k},n) = -\frac{1}{4\pi\beta e^2} \sum_{j=0}^{7} A_j(n) |\mathbf{k}|^j + o(|\mathbf{k}|^7) , \tag{2.20}$$

$$\Pi(\mathbf{k},n) = -\frac{1}{4\pi\beta e^2} \sum_{j=0}^{7} B_j(n) |\mathbf{k}|^j + o(|\mathbf{k}|^7) . \tag{2.21}$$

These expansions up to $|\mathbf{k}|^7$ do not involve any logarithmic terms or other kinds of nonanalytic terms at $\mathbf{k}=0$. The occurrence of a term $|\mathbf{k}|^j$, with j odd, or $|\mathbf{k}|^j \ln|\mathbf{k}|$, with j even ($j \geq 0$), corresponds to a spatial decay of the type $1/|\mathbf{x}|^{j+3}$. Thus the expansions (2.20) and (2.21) can only lead to algebraic decays with even powers up to $1/|\mathbf{x}|^{10}$. [The type (2.20) and (2.21) of small-$\mathbf{k}$ expansions is precisely the one obtained both from the analysis of the diagram of Fig. 3 and the class of similar graphs exhibited in Sec. III B and from the semiclassical formalism of Sec. IV.] The asymptotic behavior (2.18) imposes

$$\begin{aligned} &B_0(n) = B_1(n) = 0 , \\ &B_2(n) = \frac{1}{1+4\pi^2 n^2/(\lambda\kappa_D)^2} , \end{aligned} \tag{2.22}$$

for all $n = 0, \pm 1, \pm 2, \ldots$, while (2.19) gives the following extra information about the case $n=0$,

$$B_3(0) = 0, \quad B_4(0) = -\frac{1}{4\pi e^2 \rho \chi_T} . \tag{2.23}$$

To see the implications of (2.22) and (2.23) on (2.20), we invert the Dyson relation (2.11),

$$\Pi^*(\mathbf{k},n) = \frac{|\mathbf{k}|^2 \Pi(\mathbf{k},n)}{|\mathbf{k}|^2 + 4\pi\beta e^2 \Pi(\mathbf{k},n)} . \tag{2.24}$$

Inserting (2.18) and (2.19) into (2.24) and expanding in powers of $|\mathbf{k}|$ leads to the relations

$$A_0(0) = 4\pi e^2 \rho \chi_T > 0 , \tag{2.25}$$

and for $n = \pm 1, \pm 2, \ldots$,

$$A_0(n) = A_1(n) = 0 ,$$

$$A_2(n) = \frac{(\lambda\kappa_D)^2}{4\pi^2 n^2} = 4\pi\beta e^2 \frac{\rho\lambda^2}{4\pi^2 n^2} . \tag{2.26}$$

Moreover, one finds the following relations between the coefficients of the odd powers of $|\mathbf{k}|$ for $n=0$ [since $A_0(0) \neq 0$]:

$$\begin{aligned} B_5(0) &= \frac{A_1(0)}{[A_0(0)]^2} , \\ B_7(0) &= \frac{A_3(0)}{[A_0(0)]^2} + C^{(1)} A_1(0) , \end{aligned} \tag{2.27}$$

and for $n = \pm 1, \pm 2, \ldots$ [since $A_2(n) > 0$],

$$\begin{aligned} B_3(n) &= \frac{A_3(n)}{[A_2(n)+1]^2} , \\ B_5(n) &= \frac{A_5(n)}{[A_2(n)+1]^2} + C^{(2)} A_3(n) , \\ B_7(n) &= \frac{A_7(n)}{[A_2(n)+1]^2} + C^{(3)} A_5(n) + C^{(4)} A_3(n) . \end{aligned} \tag{2.28}$$

In (2.27) and (2.28), $C^{(r)} = 1, \ldots, 4$, are some more complicated functions of the A_j's, the exact form of which will not be relevant here.

In the following section we shall calculate the small $\mathbf{k}$ contribution to the proper polarization of the diagram of Fig. 3, the simplest graph beyond the usual RPA theory. This contribution to $A_1(0)$ is equal to zero whereas the contribution to $A_3(0)$ does not vanish, and we also show that the whole class of the higher-order ladder graphs (Fig. 4 with $N \geq 3$) does not contribute either to $A_1(0)$ or to $A_3(0)$. We then find from (2.27) that $S(\mathbf{k},n=0)$ has a dominant nonanalytic term, $S^{\text{alg}}(\mathbf{k},n=0)$, of order $|\mathbf{k}|^7$ as $|\mathbf{k}| \to 0$,

$$S^{\text{alg}}(\mathbf{k},n=0) = -\Pi^{\text{alg}}(\mathbf{k},n=0) = \frac{1}{4\pi\beta e^2} \frac{A_3(0)}{[A_0(0)]^2} |\mathbf{k}|^7 , \tag{2.29}$$

leading to a $1/|\mathbf{x}|^{10}$ decay. Moreover, the zero-frequency component of the effective potential (2.14) is nonanalytic in $\mathbf{k}$,

$$\lim_{|\mathbf{k}|\to 0} U^{\text{eff}}(\mathbf{k},n=0)\approx \frac{4\pi\beta e^2}{A_0(0)+[1+A_2(0)]|\mathbf{k}|^2+A_3(0)|\mathbf{k}|^3}, \tag{2.30}$$

with a corresponding spatial decay as $1/|\mathbf{x}|^6$, whereas, according to (2.26), the non-zero-frequency components of the effective potential are not screened and remain purely Coulombic. Finally, the small-$\mathbf{k}$ behavior of the static susceptibility (2.10) will be

$$\lim_{|\mathbf{k}|\to 0}\chi(\mathbf{k})\approx -1+\frac{1}{4\pi e^2\rho\chi_T}|\mathbf{k}|^2+\frac{1+A_2(0)}{[A_0(0)]^2}|\mathbf{k}|^4 - \frac{A_3(0)}{[A_0(0)]^2}|\mathbf{k}|^5 , \tag{2.31}$$

and $\chi(\mathbf{x})$ will decay as $1/|\mathbf{x}|^8$.

As far as the non-zero-frequency terms are concerned, the diagram of Fig. 3 gives $A_3(n)=A_5(n)=0$ but $A_7(n)\neq 0$ for $n\neq 0$, and the higher-order ladder graphs of Fig. 4 do not contribute to these coefficients. Consequently, we will have $B_3(n)=B_5(n)=0$ but $B_7(n)\neq 0$ for all $n\neq 0$, so that the dominant nonanalytic term in $S(\mathbf{k},n)$ is

$$S^{\text{alg}}(\mathbf{k},n)=-\Pi^{\text{alg}}(\mathbf{k},n) =\frac{1}{4\pi\beta e^2}\frac{A_7(n)}{[A_2(n)+1]^2}|\mathbf{k}|^7, \quad n=1,2,\ldots . \tag{2.32}$$

Thus, according to (2.9), (2.29) and (2.32) imply that $S(\mathbf{x})$ has a $1/|\mathbf{x}|^{10}$ decay.

III. THE PROPER POLARIZATION

A. Random-phase approximation

We recall here that the well-known RPA theory consists in approximating $\Pi^*(\mathbf{x},s)$ by the proper polarization diagram with the lowest order in the interaction

$$\Pi^*_{\text{RPA}}(\mathbf{x},s)=\Pi_0(\mathbf{x},s)\equiv 2G_0(\mathbf{x},s)G_0(-\mathbf{x},-s) , \tag{3.1}$$

where $G_0(\mathbf{x},s)$ is the free propagator (see Ref. [4], Sec. 23) and the factor 2 comes from the summation over the spin states. $G_0(\mathbf{x},s)$ is the inverse Fourier transform of

$$G_0(\mathbf{p},s)=e^{-(\lambda^2p^2/2-\beta\mu)s}[n_0(p)-\theta(s)] , \tag{3.2}$$

where $s=\tau/\beta\hbar$, $-1\le s\le 1$, $\theta(s)$ is the Heaviside function, and we have set $p\equiv|\mathbf{p}|$. In (3.2) $n_0(p)$ is the Fermi distribution

$$n_0(p)=\frac{1}{e^{(\lambda^2p^2/2-\beta\mu)}+1} \tag{3.3}$$

and μ is the chemical potential.

Since $G_0(\mathbf{p},s)$ is infinitely differentiable in $\mathbf{p}$, its inverse Fourier transform decays faster than any inverse power of $|\mathbf{x}|$ and so does $\Pi_0(\mathbf{x},s)$. Therefore the small-$\mathbf{k}$ expansion of $\Pi^*_{\text{RPA}}(\mathbf{k},n)$ involves only even powers of $k\equiv|\mathbf{k}|$. According to the Dyson relation (2.11) the same is true for $\Pi_{\text{RPA}}(k,n)$ and $S_{\text{RPA}}(k)$. Thus, there is no singularity at $\mathbf{k}=\mathbf{0}$ that might lead to an algebraic decay of $S_{\text{RPA}}(\mathbf{x})$.

The RPA effective potential will be used in Sec. III B. According to (2.14), it is defined by

$$U^{\text{eff}}_{\text{RPA}}(k,n)=\frac{U_0(k)}{1-U_0(k)\Pi_0(k,n)} . \tag{3.4}$$

The diagrammatic representation of this definition is shown in Fig. 1. Its small-k behavior is derived from the expansion of $\Pi_0(k,n)$ to second order in k (see Appendix A),

$$\Pi_0(k,n)=\delta_{n,0}\left[2\Gamma_2+\frac{\Gamma_3}{3}\lambda^2k^2\right] -(1-\delta_{n,0})\frac{2\Gamma_1}{4\pi^2n^2}\lambda^2k^2+O(k^4) , \tag{3.5}$$

where the coefficients Γ_N are given by integrals over derivatives of the Fermi distribution

$$\Gamma_N=\int\frac{d\mathbf{p}}{(2\pi)^3}\gamma_N(p) , \tag{3.6}$$

$$\gamma_N(p)=\frac{1}{(N-1)!}\frac{d^{N-1}}{d\zeta^{N-1}}\left[\frac{1}{e^{\zeta}+1}\right]\Bigg|_{\zeta=\lambda^2p^2/2-\beta\mu} . \tag{3.7}$$

We note in particular that

$$\Gamma_1=\int\frac{d\mathbf{p}}{(2\pi)^3}n_0(p)=\frac{\rho_0}{2} , \tag{3.8}$$

where ρ_0 is the density of the free-electron gas. Hence the small-k behavior of $U^{\text{eff}}_{\text{RPA}}(k,n)$ is given by

$$\lim_{k\to 0}U^{\text{eff}}_{\text{RPA}}(k,n)\approx\delta_{n,0}U^*_{\text{DH}}(k)+(1-\delta_{n,0})U_0(k)h(n) , \tag{3.9}$$

with

$$h(n)=\frac{1}{1+(\kappa_D^0\lambda)^2/4\pi^2n^2} , \tag{3.10}$$

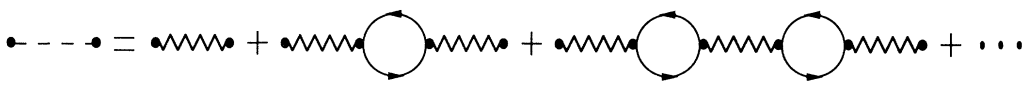

FIG. 1. RPA effective potential $U^{\text{eff}}_{\text{RPA}}$, diagrammatic representation of the definition (3.4). The potential $U^{\text{eff}}_{\text{RPA}}$ is denoted by a dotted line. As usual, a wavy line is a bare Coulomb potential and a solid line a free propagator. Then, a fermionic loop $\Pi^*_{\text{RPA}}=\Pi_0$ is represented by a directed circle.

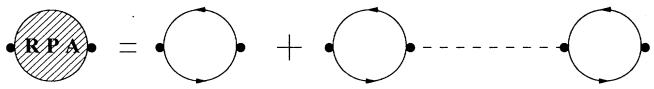

FIG. 2. Diagrammatic representation of Π_{RPA} according to the relation (2.13). Π_{RPA} is denoted by a hachured disk.

where $\kappa_D^0 \equiv \sqrt{4\pi\beta\rho_0 e^2}$ is the inverse Debye length calculated with the density ρ_0 of the free-electron gas. In (3.9), $U^*_{\mathrm{DH}}(k)$ is a generalized Debye-Hückel potential

$$U^*_{\mathrm{DH}}(k)=\frac{4\pi\beta e^{*2}}{k^2+\kappa_D^{*2}}\ , \tag{3.11}$$

with renormalized quantities

$$e^*=\left[1-(\kappa_D^0\lambda)^2\frac{\Gamma_3}{6\Gamma_1}\right]^{-1/2}e$$

and

$$\kappa_D^{*2}=4\pi\beta e^{*2}\rho^*,\quad \text{with}\quad \rho^*=\rho_0\frac{|\Gamma_2|}{\Gamma_1}\ . \tag{3.12}$$

The point is that the zero-frequency component of $U^{\mathrm{eff}}_{\mathrm{RPA}}(k,n)$ is screened as in the classical case, whereas the non-zero-frequency components remain purely Coulombic. The graphical representation of the relation (2.13) between Π_{RPA} and $U^{\mathrm{eff}}_{\mathrm{RPA}}$ is given in Fig. 2.

As a final remark, according to (3.8), the coefficient of k^2 for $n\neq 0$ in (3.5) is equal to $-\rho_0\lambda^2/4\pi^2n^2$. According to (2.26), inserting (3.5) into the Dyson relation (2.11) leads to (2.18) with ρ replaced by ρ_0: this shows that $S_{\mathrm{RPA}}(k)$ satisfies the sum rule (2.15) with the density ρ replaced by that of the noninteracting gas.

B. The proper polarization beyond the random-phase approximation

We now turn to the contribution of higher-order diagrams to the proper polarization. First we perform a partial resummation by replacing the bare interaction lines by the dotted lines of Fig. 1 associated with the RPA effective potential. As a first natural correction to (3.1), we consider the proper polarization insertion $\Pi_1^*(k,n)$ with two RPA interaction lines, given by the sum of the two topologically different diagrams displayed in Fig. 3. According to the diagrammatic rules in Fourier space (see Ref. [2] Sec. 25)

$$\Pi_1^*(k,n)=4\int\frac{d\mathbf{q}}{(2\pi)^3}\sum_{\nu=-\infty}^{+\infty}U^{\mathrm{eff}}_{\mathrm{RPA}}(\mathbf{q},\nu)U^{\mathrm{eff}}_{\mathrm{RPA}}(\mathbf{k}-\mathbf{q},n-\nu)\times\tfrac{1}{2}[\Lambda_0(\mathbf{q},\mathbf{k}-\mathbf{q},\nu,n-\nu)]^2\ , \tag{3.13}$$

where the factor 4 comes from the summation over the spin states and $\Lambda_0(\mathbf{q},\mathbf{k}-\mathbf{q},\nu,n-\nu)$ is the following symmetrized quantity associated with the electron loops of Fig. 3:

$$\Lambda_0(\mathbf{q}_1,\mathbf{q}_2,n_1,n_2)=\int\frac{d\mathbf{p}}{(2\pi)^3}\left[\sum_{m=-\infty}^{+\infty}G_0(\mathbf{p},m)G_0(\mathbf{p}+\mathbf{q}_1,m+n_1)G_0(\mathbf{p}+\mathbf{q}_1+\mathbf{q}_2,m+n_1+n_2)+\sum_{m=-\infty}^{+\infty}G_0(\mathbf{p},m)G_0(\mathbf{p}+\mathbf{q}_2,m+n_2)G_0(\mathbf{p}+\mathbf{q}_1+\mathbf{q}_2,m+n_1+n_2)\right]\ . \tag{3.14}$$

$\Lambda_0(\mathbf{q}_1,\mathbf{q}_2,n_1,n_2)$ is invariant under the simultaneous rotations of the vectors $\mathbf{q}_1$ and $\mathbf{q}_2$, symmetrical under the exchange $1\leftrightarrow 2$, and it satisfies (see Appendix B)

$$\Lambda_0(\mathbf{q}_1,\mathbf{q}_2,n_1,n_2)=\Lambda_0(\mathbf{q}_1,\mathbf{q}_2,-n_1,-n_2)\ . \tag{3.15}$$

We now investigate the long-distance behavior of $\Pi_1^*(\mathbf{x},n)$ and show that it decays algebraically. The asymptotic behavior of $\Pi_1^*(\mathbf{x},n)$ is revealed by an examination of the inverse Fourier transform of (3.13),

$$\Pi_1^*(\mathbf{x},n)=2\sum_{\nu=-\infty}^{+\infty}\int\frac{d\mathbf{q}_1}{(2\pi)^3}e^{-i\mathbf{q}_1\cdot\mathbf{x}}U^{\mathrm{eff}}_{\mathrm{RPA}}(\mathbf{q}_1,\nu)\times\int\frac{d\mathbf{q}_2}{(2\pi)^3}e^{-i\mathbf{q}_2\cdot\mathbf{x}}U^{\mathrm{eff}}_{\mathrm{RPA}}(\mathbf{q}_2,n-\nu)\times[\Lambda_0(\mathbf{q}_1,\mathbf{q}_2,\nu,n-\nu)]^2\ . \tag{3.16}$$

The possible long-range part of $\Pi_1^*(\mathbf{x},n)$ due to the

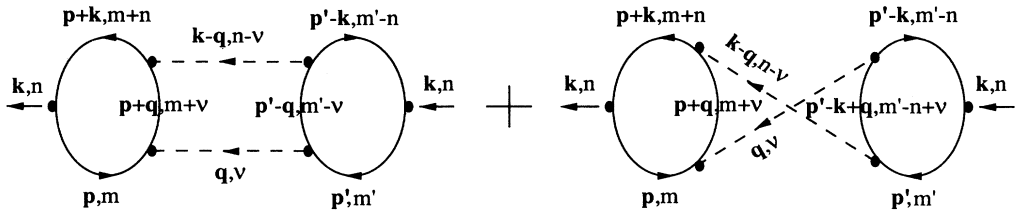

FIG. 3. Proper polarization insertion Π_1^* with two $U^{\mathrm{eff}}_{\mathrm{RPA}}$ lines. Π_1^* is the sum of the two topologically different diagrams shown in the figure. The notations are those used in (3.13).

Coulombic singularities of $U^{\text{eff}}_{\text{RPA}}(\mathbf{q},\nu)$ for $\nu\neq 0$ is governed by the behavior of the integrand of (3.16) in the neighborhood of $\mathbf{q}_1=\mathbf{q}_2=\mathbf{0}$. Thus we have to expand $\Lambda_0(\mathbf{q}_1,\mathbf{q}_2,n_1,n_2)$ for small $\mathbf{q}_1,\mathbf{q}_2$. The symmetries of $\Lambda_0(\mathbf{q}_1,\mathbf{q}_2,n_1,n_2)$ imply that this quantity is necessarily of the following form:

$$\Lambda_0(\mathbf{q}_1,\mathbf{q}_2,n_1,n_2)=\lambda_0(n_1,n_2)+\mu_1(n_1,n_2)|\mathbf{q}_1|^2 +\mu_1(n_2,n_1)|\mathbf{q}_2|^2 +\lambda_1(n_1,n_2)\mathbf{q}_1\cdot\mathbf{q}_2+\cdots , \tag{3.17}$$

where the ellipsis represents terms of higher order formed with $|\mathbf{q}_1|^2$, $|\mathbf{q}_2|^2$, and $\mathbf{q}_1\cdot\mathbf{q}_2$. Any term occurring in $[\Lambda(\mathbf{q}_1,\mathbf{q}_2,\nu,n-\nu)]^2$ with $\nu\neq 0$ and that has a power of $|\mathbf{q}_1|^2$ as a factor cancels the Coulombic singularity of $U^{\text{eff}}_{\text{RPA}}(\mathbf{q}_1,\nu)$. These terms do not contribute to the long-distance behavior since they involve $\Delta 1/|\mathbf{x}|$, which is local. The same is true for the terms in $[\Lambda_0(\mathbf{q}_1,\mathbf{q}_2,\nu,n-\nu)]^2$ with $n\neq\nu$ and having a power of $|\mathbf{q}_2|^2$ as a factor. Moreover, according to (3.9), any term in $[\Lambda_0(\mathbf{q}_1,\mathbf{q}_2,\nu,n-\nu)]^2$ with $\nu=0$ or $\nu=n$ is associated in (3.16) with a Debye-Hückel potential or its derivatives. Hence these terms do not lead to an algebraic decay either. Therefore, the only part of $\Lambda_0(\mathbf{q}_1,\mathbf{q}_2,\nu,n-\nu)$ that contributes to the algebraic decay of $\Pi^*(\mathbf{x},n)$ is

$$\Lambda_0^{\text{alg}}(\mathbf{q}_1,\mathbf{q}_2,\nu,n-\nu)=\sum_{j\geq 0}\lambda_j(\nu,n-\nu)(\mathbf{q}_1\cdot\mathbf{q}_2)^j , \tag{3.18}$$

with $\nu\neq 0$ and $\nu\neq n$.

According to the results (B8) of Appendix B, one has, if $n=0$ and $\nu\neq 0$,

$$\lambda_0(\nu,-\nu)=0,\quad \lambda_1(\nu,-\nu)=\lambda^2\frac{\Gamma_2}{4\pi^2\nu^2} , \tag{3.19}$$

and, if $n\neq 0$, $\nu\neq 0$ and $n-\nu\neq 0$,

$$\lambda_0(\nu,n-\nu)=0,\quad \lambda_1(\nu,n-\nu)=0 ,$$
$$\lambda_2(\nu,n-\nu)=\lambda^4\frac{1}{4\pi^2n^2}\left[\frac{2\Gamma_1}{4\pi^2n\nu}+\frac{2\Gamma_1}{4\pi^2n(n-\nu)}\right] . \tag{3.20}$$

Therefore the dominant algebraic contribution to $\Pi_1^*(\mathbf{x},n)$ is

$$\Pi_1^{*\text{alg}}(\mathbf{x},n=0)=a_3(0)\int\frac{d\mathbf{q}_1}{(2\pi)^3}\int\frac{d\mathbf{q}_2}{(2\pi)^3}e^{-i(\mathbf{q}_1+\mathbf{q}_2)\cdot\mathbf{x}}\frac{(\mathbf{q}_1\cdot\mathbf{q}_2)^2}{|\mathbf{q}_1|^2|\mathbf{q}_2|^2}=\frac{6}{(4\pi)^2}a_3(0)\frac{1}{|\mathbf{x}|^6} \tag{3.21}$$

and, for $n\neq 0$,

$$\Pi_1^{*\text{alg}}(\mathbf{x},n)=a_7(n)\int\frac{d\mathbf{q}_1}{(2\pi)^3}\int\frac{d\mathbf{q}_2}{(2\pi)^3}e^{-i(\mathbf{q}_1+\mathbf{q}_2)\cdot\mathbf{x}}\frac{(\mathbf{q}_1\cdot\mathbf{q}_2)^4}{|\mathbf{q}_1|^2|\mathbf{q}_2|^2}=\frac{7!}{2}\frac{1}{(4\pi)^2}a_7(n)\frac{1}{|\mathbf{x}|^{10}} , \tag{3.22}$$

with

$$a_3(0)=2(4\pi\beta e^2)^2\sum_{\substack{\nu=-\infty\\ \nu\neq 0}}^{+\infty}h^2(\nu)\lambda_1^2(\nu,-\nu) , \tag{3.23}$$

$$a_7(n)=2(4\pi\beta e^2)^2\sum_{\substack{\nu=-\infty\\ \nu\neq 0,n}}^{+\infty}h(\nu)h(n-\nu)\lambda_2^2(\nu,n-\nu) , \tag{3.24}$$

where $h(\nu)$ is defined in (3.10). Hence, by using the Fourier transforms $(\pi^2/12)|\mathbf{k}|^3$ and $(2\pi^2/8!)|\mathbf{k}|^7$ of $|\mathbf{x}|^{-6}$ and $|\mathbf{x}|^{-10}$, we find that the dominant nonanalytic part of $\Pi_1^*(\mathbf{k},n)$ for small $\mathbf{k}$ is

$$\Pi_1^{*\text{alg}}(\mathbf{k},n)=\delta_{n,0}\tfrac{1}{32}a_3(0)|\mathbf{k}|^3 +(1-\delta_{n,0})\frac{1}{(32)(4)}a_7(n)|\mathbf{k}|^7 . \tag{3.25}$$

Since the coefficients $a_3(0)$ and $a_7(n)$ are obviously different from zero, we see that the graph of Fig. 3 gives nonvanishing contributions to the coefficients $A_3(0)$ and $A_7(n)$ of the expansion (2.20); hence the conclusions (2.29)–(2.32) of the preceding section are true, as far as the graph of Fig. 3 is concerned.

We now comment on a larger class of graphs, the ladder graphs, which are the generalization of Fig. 3 with N effective interaction lines (see Fig. 4). Up to a numerical factor, the contribution of such a graph to $\Pi^*(\mathbf{x},n)$ has the following form [similar to (3.16)].

$$\sum_{\substack{n_1,\ldots,n_N\\ n_1+\ldots+n_N=n}}\int\frac{d\mathbf{q}_1}{(2\pi)^3}e^{-i\mathbf{q}_1\cdot\mathbf{x}}U^{\text{eff}}_{\text{RPA}}(\mathbf{q}_1,n_1)\cdots \times\int\frac{d\mathbf{q}_N}{(2\pi)^3}e^{-i\mathbf{q}_N\cdot\mathbf{x}}U^{\text{eff}}_{\text{RPA}}(\mathbf{q}_N,n_N) \times[\Lambda_0(\mathbf{q}_1,\ldots,\mathbf{q}_N,n_1,\ldots,n_N)]^2 . \tag{3.26}$$

$\Lambda_0(\mathbf{q}_1,\ldots,\mathbf{q}_N,n_1,\ldots,n_N)$ is the contribution of the fermionic loops of Fig. 4,

$$\Lambda_0(\mathbf{q}_1,\ldots,\mathbf{q}_N,n_1,\ldots,n_N)=\int\frac{d\mathbf{p}}{(2\pi)^3}\sum_{\pi\in\Pi_N}G_0(\mathbf{p},m)G_0(\mathbf{p}+\mathbf{q}_{\pi_1},m+n_{\pi_1})\cdots \times G_0(\mathbf{p}+\mathbf{q}_{\pi_1}+\cdots+\mathbf{q}_{\pi_N},m+n_{\pi_1}+\cdots+n_{\pi_N}) , \tag{3.27}$$

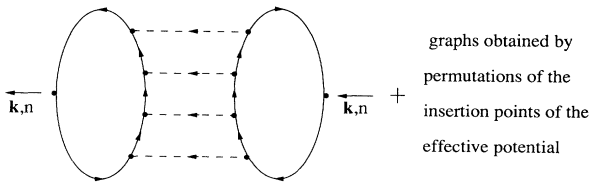

FIG. 4. Ladder graph: proper polarization insertion with N $U^{\text{eff}}_{\text{RPA}}$ lines.

where Π_N is the group of the permutations of $\{1,\ldots,N\}$. The most singular part of the integrand of (3.26) comes again from the non-zero-frequency terms in the neighborhood of $\mathbf{q}_1=\cdots=\mathbf{q}_N=\mathbf{0}$. Expanding $\Lambda_0(\mathbf{q}_1,\ldots,\mathbf{q}_N,n_1,\ldots,n_N)$ for small $\mathbf{q}_1,\ldots,\mathbf{q}_N$, we show in Appendix C that $\Lambda_0^{\text{alg}}(\mathbf{q}_1,\ldots,\mathbf{q}_N,n_1,\ldots,n_N)$, the only part of $\Lambda_0(\mathbf{q}_1,\ldots,\mathbf{q}_N,n_1,\ldots,n_N)$ that contributes to the algebraic decay of (3.26), has the following structure for $N\geq 3$:

$$\Lambda_0^{\text{alg}}(\mathbf{q}_1,\ldots,\mathbf{q}_N,n_1,\ldots,n_N)=\lambda_0\delta_{n_1,0}\cdots\delta_{n_N,0}+\sum_{\substack{i,j\\ i\neq j}}\mathbf{q}_i\cdot\mathbf{q}_j\lambda_1(n_i,n_j)\times\prod_{k\neq i,j}\delta_{n_k,0}+\cdots, \tag{3.28}$$

where the ellipsis represents terms of higher order formed with the $\mathbf{q}_i\cdot\mathbf{q}_j$'s. So, if $N\geq 3$, the nonzero frequencies may simultaneously occur only at the eighth order in the expansion of $[\Lambda_0^{\text{alg}}(\mathbf{q}_1,\ldots,\mathbf{q}_N,n_1,\ldots,n_N)]^2$. Then, by a simple scaling argument, we see that (3.26) decays at least as $1/|\mathbf{x}|^{N+8}$. Hence, for $N\geq 3$, these ladder diagrams give no contribution either to the coefficients $A_1(0)$ and $A_3(0)$ or to the coefficients $A_3(n)$, $A_5(n)$, and $A_7(n)$ for $n\neq 0$ in the small-$\mathbf{k}$ expansion of $\Pi^*(\mathbf{k},n)$. We conclude that the behaviors (2.29)–(2.32) remain the same when all the ladder diagrams are taken into account. Of course, to establish the full validity of the behaviors (2.29)–(2.32), it would be necessary to examine all the higher-order proper polarization parts, a fairly complex task. In the following section, we investigate the same problem in the simpler semiclassical regime where the effects of the Fermi statistics are neglected.

IV. BOLZTMANN ELECTRON GAS

A. Statistical mechanical system of charged filaments

The most convenient way to study the correlations of a quantum Coulomb gas with Boltzmann statistics is by the functional integration formalism [7,1]. In this representation, to each quantum charge is associated a closed random path $\xi(s)$, $0\leq s\leq 1$, $\xi(0)=\xi(1)=0$ (a Brownian bridge) having a Gaussian probability measure $D(\xi)$ normalized to one, with a zero mean and a covariance equal to

$$\langle[\xi(s_1)]_\alpha[\xi(s_2)]_\beta\rangle=\int D(\xi)[\xi(s_1)]_\alpha[\xi(s_2)]_\beta=\delta_{\alpha,\beta}\begin{cases}s_1(1-s_2) & \text{if } s_1\leq s_2\\ s_2(1-s_1) & \text{if } s_2\leq s_1\end{cases}, \tag{4.1}$$

$\alpha,\beta=1,2,3$, where $[\xi(s_1)]_\alpha$ is the α component of $\xi(s_1)$. The pair interaction between two electrons $(\mathbf{x}_i,\xi_i)$ at position $\mathbf{x}_i$ and with path ξ_i $(i=1,2)$ is given by the ξ-dependent potential

$$\phi(\mathbf{x}_1-\mathbf{x}_2,\xi_1,\xi_2)=\int_0^1 ds\; U_0(\mathbf{x}_1-\mathbf{x}_2+\lambda\xi_1(s)-\lambda\xi_2(s)), \tag{4.2}$$

where $U_0(\mathbf{x})=\beta e^2/|\mathbf{x}|$ is equal to β times the Coulomb potential (as in Sec. II) and $\lambda=\hbar\sqrt{\beta/m}$ is the de Broglie thermal wavelength. One can thus visualize the quantum system of point electrons as an equivalent classical gas of charged random filaments, and apply to it the methods of classical statistical mechanics. The state of a filament is specified by its position $\mathbf{x}$ and by the internal degree of freedom ξ associated with its shape. Two filaments interact by means of the potential (4.2), and integrations over phase space run on all positions and internal degrees of freedom with the measure $D(\xi)$. Moreover a filament has two spin states, but, since the interaction does not depend on them, they will only lead to a degeneracy factor equal to 2.

From this point on, we can proceed exactly as in the Mayer graph summation for a classical plasma [8,9]. The grand canonical truncated pair correlation function reads

$$\rho_T(\mathbf{x}_1-\mathbf{x}_2)=\int D(\xi_1)D(\xi_2)\rho_T(\mathbf{x}_1,\xi_1,\mathbf{x}_2,\xi_2), \tag{4.3}$$

where $\rho_T(\mathbf{x}_1,\xi_1,\mathbf{x}_2,\xi_2)$ can be expressed as the usual sum of cluster integrals

$$\rho_T(1,2)=\sum_{N=0}^{\infty}\frac{(2z)^{N+2}}{N!}I_N(1,2) \tag{4.4}$$

where the factor 2 comes from the summation over the spin states and $I_0(1,2)=f(1,2)$ while, for $N\geq 1$,

$$I_N(1,2)=\sum_{G\in\Gamma_N}\int d3\ldots d(N+2)\prod_{(i,j)}f(i,j). \tag{4.5}$$

In (4.4) and (4.5), $i\equiv(\mathbf{x}_i,\xi_i)$ denotes the filament variables and $di\equiv\int d\mathbf{x}_i\int D(\xi_i)$ is the corresponding phase-space integration. The sum runs on the set Γ_N of all the labeled connected graphs with two root points 1,2 and N internal points. Each pair of points is linked by at most one f bond,

$$f(i,j)\equiv e^{-\phi(i,j)}-1, \tag{4.6}$$

where $\phi(i,j)$ is the potential (4.2). As in classical physics, the activity z is related to the chemical potential μ by $z=e^{\beta\mu}/(2\pi\lambda^2)^{3/2}$. The f bonds can be expanded into ϕ_k bonds

$$f(i,j)=\sum_{k=1}^{\infty}(-1)^k\phi_k(i,j) \tag{4.7}$$

with

$$\phi_k(i,j)\equiv\frac{1}{k!}[\phi(i,j)]^k \ . \tag{4.8}$$

A ϕ_k bond is represented by k potential lines joining i and j as shown in Fig. 5. The difference between graphs composed of f bonds and ϕ_k bonds is that in the latter case an arbitrary number of potential lines between each pair of points is permitted.

Then one defines the quantum effective potential $\phi^{\text{eff}}(\mathbf{x}_1-\mathbf{x}_2,\xi_1,\xi_2)$ by the chain summation of ϕ_1 bonds represented in Fig. 6:

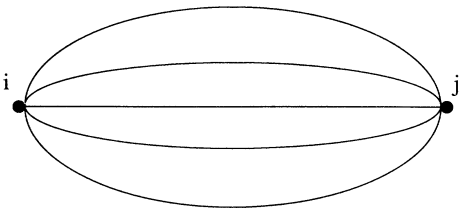

FIG. 5. ϕ_k bond (4.8) with k $\phi=\phi_1$ lines (4.2). The potential ϕ is denoted by a solid line and its arguments $i=(\mathbf{y}_i,\alpha_i)$ and $j=(\mathbf{y}_j,\alpha_j)$, where both the $\mathbf{x}$'s and the α s are to be integrated-over, by black points.

$$\phi^{\text{eff}}(\mathbf{x}_1-\mathbf{x}_2,\xi_1,\xi_2)=\phi(\mathbf{x}_1-\mathbf{x}_2,\xi_1,\xi_2)+\sum_{N=1}^{\infty}(-2z)^N\int d\mathbf{y}_1\ldots d\mathbf{y}_N\int D(\alpha_1)\ldots D(\alpha_N)\times\phi(\mathbf{x}_1-\mathbf{y}_1,\xi_1,\alpha_1)\phi(\mathbf{y}_1-\mathbf{y}_2,\alpha_1,\alpha_2)\ldots\phi(\mathbf{y}_N-\mathbf{x}_2,\alpha_N,\xi_2) \ . \tag{4.9}$$

The main properties of $\phi^{\text{eff}}(\mathbf{x}_2-\mathbf{x}_2,\xi_1,\xi_2)$ are established in Appendix C. In particular, its Fourier transform is given by (C12)

$$\phi^{\text{eff}}(\mathbf{k},\xi_1,\xi_2)=\int_0^1 ds_1\int_0^1 ds_2 e^{-i\lambda\mathbf{k}\cdot[\xi_1(s_1)-\xi_2(s_2)]}\tilde{U}^{\text{eff}}_{\text{RPA}}(\mathbf{k},s_1-s_2)$$
$$=\int_0^1 ds_1\int_0^1 ds_2 e^{-i\lambda\mathbf{k}\cdot[\xi_1(s_1)-\xi_2(s_2)]}\sum_{n=-\infty}^{\infty}e^{-i2\pi n(s_1-s_2)}\tilde{U}^{\text{eff}}_{\text{RPA}}(\mathbf{k},n) \ , \tag{4.10}$$

where $\tilde{U}^{\text{eff}}_{\text{RPA}}(\mathbf{k},n)$, defined in (C11), is the limit of $U^{\text{eff}}_{\text{RPA}}(\mathbf{k},n)$ when the Fermi statistics is suppressed. Subsequently $\phi^{\text{eff}}(\mathbf{x},\xi_1,\xi_2)$ can be split as $U^{\text{eff}}_{\text{RPA}}(\mathbf{x},n)$ into a short-range part corresponding to the $n=0$ term in (4.10) and a long-range part [$n\neq 0$ terms in (4.10)],

$$\phi^{\text{eff}}(\mathbf{x},\xi_1,\xi_2)=\phi^{\text{eff}}_S(\mathbf{x},\xi_1,\xi_2)+\phi^{\text{eff}}_L(\mathbf{x},\xi_1,\xi_2) \ . \tag{4.11}$$

The short-range part decays faster than any inverse power of the distance, while, for fixed ξ_1 and ξ_2 the long-range part behaves as a dipolar potential [see (C20)],

$$\lim_{|\mathbf{x}|\to\infty}\phi^{\text{eff}}_L(\mathbf{x},\xi_1,\xi_2)\approx-\lambda^2\beta e^2\int_0^1 ds_1\int_0^1 ds_2\tilde{h}(s_1-s_2)[\xi_1(s_1)\cdot\nabla][\xi_2(s_2)\cdot\nabla]\frac{1}{|\mathbf{x}|} \ , \tag{4.12}$$

where

$$\tilde{h}(s)=\sum_{\substack{n=-\infty\\ n\neq 0}}^{\infty}e^{-2i\pi ns}\tilde{h}(n)$$

and $\tilde{h}(n)$ is given by (C17). However, after integrating over either ξ_1 or ξ_2, one finds that the potentials

$$\phi^{\text{eff}}(\mathbf{x},\xi_1)\equiv\int D(\xi_2)\phi^{\text{eff}}(\mathbf{x},\xi_1,\xi_2)$$

and

$$\phi^{\text{eff}}(\mathbf{x},\xi_2)\equiv\int D(\xi_1)\phi^{\text{eff}}(\mathbf{x},\xi_1,\xi_2)$$

are again short ranged (see the end of Appendix C).

In particular, the correlation calculated with the chain approximation

$$\rho_T^{\text{chain}}(\mathbf{x}_1,\mathbf{x}_2)\equiv-\tilde{\rho}_0^2\int D(\xi_1)\int D(\xi_2)\phi^{\text{eff}}(\mathbf{x}_1-\mathbf{x}_2,\xi_1,\xi_2) \tag{4.13}$$

is rapidly decreasing. [In (4.13) $\tilde{\rho}_0=2z$ is the density of the system of noninteracting filaments with Boltzmann statistics.] Another way of proving this fast decay is to note that $S^{\text{chain}}(k)\equiv\tilde{\rho}_0+\rho_T^{\text{chain}}(k)$ coincides with $\tilde{S}_{\text{RPA}}(k)$, the limit of the RPA structure factor when the Fermi

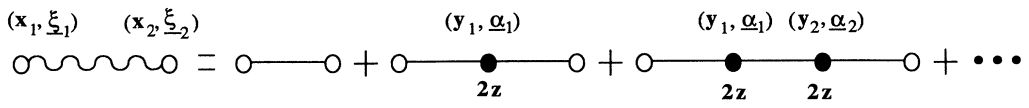

FIG. 6. Effective potential ϕ^{eff} obtained by the chain summation of ϕ bonds defined in (4.9). An effective interaction ϕ^{eff} is denoted by a wiggly line and a root point $(\mathbf{x}_i,\xi_i)$, where only ξ_i is to be integrated over, by a white point, A weight $2z$ is associated with each black point.

statistics are suppressed.

$$S^{\text{chain}}(k)=\tilde{S}_{\text{RPA}}(k) . \tag{4.14}$$

Indeed, according to (2.9), (2.13), and (3.1), $\tilde{S}_{\text{RPA}}(k)$ reads

$$\tilde{S}_{\text{RPA}}(k)=-\tilde{\Pi}_0(k,s=0) - \int_0^1 ds_1 \int_0^1 ds_2 \tilde{\Pi}_0(k,s_1) \times \tilde{U}^{\text{eff}}_{\text{RPA}}(k,s_1-s_2)\tilde{\Pi}_0(k,-s_2) , \tag{4.15}$$

where $\tilde{\Pi}_0(k,s)$ is the Boltzmann limit of $\Pi_0(k,s)$ studied in Appendix C. Inserting the expression of (C5) and (C11) into (4.15), we easily verify (4.14). Then, since $S_{\text{RPA}}(\mathbf{x})$ is rapidly decreasing, so do $\tilde{S}_{\text{RPA}}(\mathbf{x})$ and $\rho_T^{\text{chain}}(\mathbf{x})$. Finally, we note that in the classical limit $\tilde{S}_{\text{RPA}}(k)$ reduces to the Debye-Hückel form $S_{\text{DH}}(k)$,

$$\lim_{\hbar\to 0}\tilde{S}_{\text{RPA}}(k)=S_{\text{DH}}(k)=\tilde{\rho}_0-\tilde{\rho}_0^2\tilde{U}_{\text{DH}}(k) . \tag{4.16}$$

Indeed, in this limit $\tilde{\Pi}_0(k,s)$ tends to $-\tilde{\rho}_0$ for any s [see (C7) when $\lambda\to 0$] while $\tilde{U}^{\text{eff}}_{\text{RPA}}(k,n=0)=\phi^{\text{eff}}(k,n=0)$ goes to $\tilde{U}_{\text{DH}}(k)$ given by (C21) and (4.15) becomes equal to $S_{\text{DH}}(k)$.

However the representation of the quantum electron gas in terms of classical charged random filaments enables us to clearly exhibit the dipolar nature of the system. When all chain resummations have been performed, the cluster expansion of $\rho_T(1,2)$ is restricted to the so-called prototype graphs [8,9], where all lines correspond now to the effective potential (4.9). Prototype graphs are characterized by the fact that at least three effective potential lines are attached to every point, except possibly to the root points. The simplest diagram showing an algebraic decay due to the underlying effective dipolar forces (4.12) is the two bond graph shown in Fig. 7. The contribution of this graph to (4.4) is equal [up to a factor $(2z)^2$] to

$$V_2(\mathbf{x}_1-\mathbf{x}_2,\xi_1,\xi_2)\equiv\tfrac{1}{2}[\phi^{\text{eff}}(\mathbf{x}_1-\mathbf{x}_2,\xi_1,\xi_2)]^2 . \tag{4.17}$$

According to (4.11),

$$V_2(\mathbf{x})\equiv\int D(\xi_1)\int D(\xi_2)V_2(\mathbf{x},\xi_1,\xi_2)$$

behaves asymptotically as

$$\lim_{|\mathbf{x}|\to\infty} V_2(\mathbf{x})\approx\tfrac{1}{2}\int D(\xi_1)\int D(\xi_2)[\phi_L^{\text{eff}}(\mathbf{x}_1-\mathbf{x}_2,\xi_1,\xi_2)]^2 \tag{4.18}$$

Using (4.12) and the rules of Gaussian measures (4.1), we get $V_2^{\text{alg}}(\mathbf{x})$, the dominant term in the asymptotic behavior of $V_2(\mathbf{x})$,

$$V_2^{\text{alg}}(\mathbf{x})\equiv\lambda^4\frac{\beta^2e^4}{2}\int D(\xi_1)\int D(\xi_2)\left[\int_0^1 ds_1\int_0^1 ds_2\tilde{h}(s_1-s_2)[\xi_1(s_1)\cdot\nabla][\xi_2(s_2)\cdot\nabla]\frac{1}{|\mathbf{x}|}\right]^2$$
$$=\lambda^4\frac{\beta^2e^4}{2}\left[\sum_{\substack{\nu=-\infty\\ \nu\neq 0}}^{+\infty}\frac{\tilde{h}^2(\nu)}{(4\pi^2\nu^2)^2}\right]\sum_{\alpha,\beta}\left[\frac{\partial^2}{\partial x_\alpha\partial x_\beta}\left[\frac{1}{|\mathbf{x}|}\right]\right]^2 . \tag{4.19}$$

In (4.19) we have used the properties $\tilde{h}(\nu=0)=0$, $\tilde{h}(\nu)=\tilde{h}(-\nu)$, and

$$\int_0^1 ds_1\int_0^1 ds_1'\langle[\xi_1(s_1)]_\alpha[\xi(s_1')]_{\alpha'}\rangle e^{i2\pi(\nu s_1+\nu' s_1')}=\delta_{\alpha,\alpha'}\frac{\delta_{\nu,-\nu'}}{4\pi^2\nu^2}$$

if $\nu\neq 0$ and $\nu'\neq 0$. Since

$$\sum_{\alpha,\beta}\left[\frac{\partial^2}{\partial x_\alpha\partial x_\beta}\left[\frac{1}{|\mathbf{x}|}\right]\right]^2=\frac{6}{|\mathbf{x}|^6} ,$$

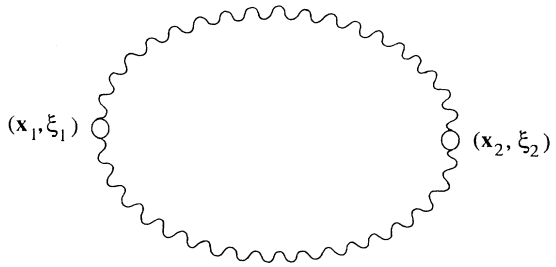

FIG. 7. V_2 bond ($=\phi_2^{\text{eff}}$ bond) with two ϕ^{eff} lines (4.9).

then

$$V_2^{\text{alg}}(\mathbf{x})=\frac{B}{|\mathbf{x}|^6} , \tag{4.20}$$

where B is a positive coefficient,

$$B=\hbar^4\left[\frac{\beta^2e^2}{m}\right]^2 3\sum_{\substack{\nu=-\infty\\ \nu\neq 0}}^{+\infty}\frac{\tilde{h}^2(\nu)}{(4\pi^2\nu^2)^2} . \tag{4.21}$$

Equivalently, $V_2^{\text{alg}}(\mathbf{k})$, the dominant nonanalytic part of the Fourier transform of $V_2(\mathbf{x})$, behaves as $|\mathbf{k}|^3$,

$$V_2^{\text{alg}}(\mathbf{k})=B\frac{\pi^2}{12}|\mathbf{k}|^3 . \tag{4.22}$$

We note that if the Fermi statistics are neglected, the $|\mathbf{k}|^3$ term in the expression (3.25) of $\tilde{\Pi}_1^{*\text{alg}}(\mathbf{k},n=0)$ agrees with (4.22), i.e.,

$$\tilde{\Pi}_1^{*\text{alg}}(\mathbf{k},n=0)=\tilde{\rho}_0^2V_2^{\text{alg}}(\mathbf{k}) . \tag{4.23}$$

Indeed, let us consider the limit of the Boltzmann statistics for $\Pi_1^*(\mathbf{k},n=0)$ defined in (3.13). In this regime

$\tilde{U}^{\rm eff}_{\rm RPA}(\mathbf{q},\nu)=\phi^{\rm eff}(\mathbf{q},\nu)$ and, if $\nu\neq 0$, its small-$\mathbf{q}$ behavior is

$$\lim_{|\mathbf{q}|\to 0}\phi^{\rm eff}(\mathbf{q},\nu)\approx\tilde{h}(\nu)U_0(\mathbf{q})$$

[see (C15)], while, according to (C13), $\lambda_1(\nu,-\nu)$ given by (3.19) tends to $-\frac{1}{2}\tilde{\rho}_0\lambda^2/4\pi^2\nu^2$. Hence, in this limit the dominant nonanalytic part of the small-$\mathbf{k}$ behavior of $\tilde{\Pi}^*_1(\mathbf{k},n=0)$ is

$$\tilde{\Pi}^{*\rm alg}_1(\mathbf{k},n=0)=\tilde{\rho}_0^2\frac{\lambda^4}{2}\left[\sum_{\substack{\nu=-\infty\\ \nu\neq 0}}^{+\infty}\frac{\tilde{h}^2(\nu)}{(4\pi^2\nu^2)^2}\right]\times\int\frac{d\mathbf{q}}{(2\pi)^3}\frac{(4\pi\beta e^2)^2}{\mathbf{q}^2(\mathbf{k}-\mathbf{q})^2}[\mathbf{q}\cdot(\mathbf{k}-\mathbf{q})]^2\ , \tag{4.24}$$

which is identical to (4.19) in Fourier space (up to a factor $\tilde{\rho}_0^2$).

Moreover, the algebraic decay (4.20) occurs at the order $\hbar^4$. Therefore, to calculate B at this order, it suffices to replace $\tilde{h}(\nu)$ by its classical value 1 (obtained by setting $\lambda\tilde{\kappa}^0_D=0$ in (C17)]. Since $\sum_{\substack{\nu=-\infty\\ \nu\neq 0}}^{+\infty}1/(4\pi^2\nu^2)^2=1/(8)(90)$,

$$B=\frac{\hbar^4}{240}\frac{(\beta e)^4}{m^2}+o(\hbar^4)\ , \tag{4.25}$$

which is exactly the formula (7.27) of Ref. [1].

At this point, we could study the effect of the insertion of the diagram of Fig. 7 on the asymptotic behavior of ρ_T in the Boltzmann regime, as we treated the effect of the proper polarization insertion of Fig. 3 on S in the quantum many-body perturbation theory (see Sec. II). We rather show that the single diagram of Fig. 7 determines the exact asymptotic behavior of ρ_T in the semiclassical limit (i.e., at the order $\hbar^4$ in the Planck constant).

B. Exact summation in the semiclassical limit

In this subsection, we calculate the exact asymptotic behavior of the pair correlation (4.3) at the order h^4 in the Planck constant. The general strategy is as follows. We first expand the $\phi^{\rm eff}_k$ bond occurring in prototype graphs in powers of $\hbar$

$$\phi^{\rm eff}_k(i,j)\equiv\frac{1}{k!}[\phi^{\rm eff}(i,j)]^k\equiv\sum_{n=0}^{+\infty}\hbar^n\phi^{{\rm eff}(n)}_k(i,j)\ . \tag{4.26}$$

In particular, $\phi^{\rm eff}(i,j)=\phi^{\rm eff}_1(i,j)=\sum_{n=0}^{+\infty}\hbar^n\phi^{{\rm eff}(n)}_1(i,j)$ and so

$$\phi^{\rm eff}_k(i,j)=\frac{1}{k!}\left[\sum_{n=0}^{+\infty}\hbar^n\phi^{{\rm eff}(n)}_1(i,j)\right]^k\ . \tag{4.27}$$

We call $(\hbar^n,k)$ bond (or simply $\hbar^n$ bond) the contribution (4.26) of order $\hbar^n$ to a $\phi^{\rm eff}_k$ bond (i,j). The bonds $\phi^{{\rm eff}(0)}_k$ of order zero are called classical. Then, in order to examine the behavior of a prototype graph at a given order m, it suffices to consider all the ways of placing $\hbar^n$ bonds, $0\leq n\leq m$, in such a way that the overall power of $\hbar$ is precisely equal to m. For instance, a prototype graph at order $\hbar^2$ is the sum of all the contributions of the same prototype graph having exactly either one $\hbar^2$ bond or two $\hbar$ bonds.

We say that a $\hbar^n$ bond is fast if $\phi^{{\rm eff}(n)}_k(\mathbf{x}_1-\mathbf{x}_2,\xi_1,\xi_2)$ decays faster than any inverse power of the distance $|\mathbf{x}_1-\mathbf{x}_2|$. We also say that a $\hbar^n$ bond (i,j) has a *classical end* if the point i (or j) is such that all other effective potential lines attached to it are classical and so do not depend on ξ_i (or ξ_j), as it will be checked in (4.28).

We first consider the $(\hbar^n,1)$ bonds. Expanding the effective potential in powers of $\hbar$, one obtains from (C21) and (C22) that the classical limit of $\phi^{\rm eff}(\mathbf{x},\xi_1,\xi_2)$ is equal to the Debye-Hückel potential (independent of ξ_1 and ξ_2) associated with the density $\tilde{\rho}_0$,

$$\phi^{{\rm eff}(0)}_1(\mathbf{x},\xi_1,\xi_2)=\tilde{U}_{\rm DH}(\mathbf{x}) \tag{4.28}$$

and the term in $\phi^{\rm eff}(\mathbf{x},\xi_1,\xi_2)$ which is linear in $\hbar$ is

$$\phi^{{\rm eff}(1)}_1(\mathbf{x},\xi_1,\xi_2)=\left[\frac{\beta}{m}\right]^{1/2}\int_0^1 ds[\xi_1(s)-\xi_2(s)]\cdot\nabla\tilde{U}_{\rm DH}(\mathbf{x})\ . \tag{4.29}$$

Thus, the $(\hbar^n,1)$ bonds are fast for $n=0,1$. On the other hand, (4.12) shows that the $(\hbar^n,1)$ bonds, $n\geq 2$ may have a dipolar asymptotic behavior. In particular, the asymptotic form of $(\hbar^2,1)$ bonds is given by (4.12) where $\tilde{h}(s)$ is replaced by its classical limit $\delta(s)-1$[see (C17)],

$$\lim_{|\mathbf{x}|\to\infty}\phi^{{\rm eff}(2)}_1(\mathbf{x},\xi_1,\xi_2)\approx-\frac{\beta^2e^2}{m}\int_0^1 ds_1\int_0^1 ds_2[\delta(s_1-s_2)-1][\xi_1(s_1)\cdot\nabla][\xi_2(s_2)\cdot\nabla]\frac{1}{|\mathbf{x}|}\ . \tag{4.30}$$

However, all the $(\hbar^n,1)$ bonds are fast when integrated on at least one of the internal variables ξ_1 of ξ_2, as a consequence of the same property for the full effective potential $\phi^{\rm eff}(\mathbf{x},\xi_1,\xi_2)$ (see the final remark of Appendix C).

The properties of the $(\hbar^n,k)$ bonds for $k\geq 2$ follow directly from the expansion of (4.27) combined with the fact that the bonds (4.28) and (4.29) are fast. When $k\geq 2$ and $n\leq 4$, one finds that all $(\hbar^n,k)$ bonds except for the $(\hbar^4,2)$ bond are fast, because all these bonds involve at least one of the rapidly decreasing quantities (4.28) or (4.29) as a factor. The $(\hbar^4,2)$ bond in turn is algebraic. The dominant algebraic decay of $\phi^{\rm eff}_2(i,j)=\frac{1}{2}[\phi^{\rm eff}(i,j)]^2$ at the order $\hbar^4$ comes from the square of the term of order $\hbar^2$ in (4.12), i.e.,

$$\lim_{|\mathbf{x}|\to\infty}\phi^{{\rm eff}(4)}_2(\mathbf{x},\xi_1,\xi_2)\approx\tfrac{1}{2}[\phi^{{\rm eff}(2)}_1(\mathbf{x},\xi_1,\xi_2)]^2\ . \tag{4.31}$$

Note that, according to the definitions (4.17) and (4.26), $\phi^{\rm eff}_2(i,j)=V_2(i,j)$ and the dominant algebraic decay of $\phi^{{\rm eff}(4)}_2$ is equal to $V^{{\rm alg}(4)}_2(\mathbf{x},\xi_1,\xi_2)$, the term of order $\hbar^4$ in $V^{\rm alg}_2(\mathbf{x},\xi_1,\xi_2)$ defined in (4.19),

$$\lim_{|\mathbf{x}|\to\infty} \hbar^4 \phi_2^{\mathrm{eff}(4)}(\mathbf{x},\xi_1,\xi_2) \approx V_2^{\mathrm{alg}(4)}(\mathbf{x},\xi_1,\xi_2)$$
$$= \hbar^4 \frac{1}{2}\left[\frac{\beta^2 e^2}{m}\right]^2 \left[\int_0^1 ds_1 \int_0^1 ds_2 [\delta(s_1-s_2)-1][\xi_1(s_1)\cdot\nabla][\xi_2(s_2)\cdot\nabla]\frac{1}{|\mathbf{x}|}\right]^2 . \quad (4.32)$$

With this information, we can study the semiclassical properties of a prototype graph (integrated on all the ξ variables, including those of the root points). We first note that the $\hbar$ expansion of a prototype graph is necessarily even. Indeed, an odd term can only originate from the expansion of $e^{i\lambda\mathbf{k}\cdot[\xi_1(s_1)-\xi_2(s_2)]}$ in the effective potential (4.10). This term is necessarily also odd in ξ, and so vanishes after integration in ξ because of the symmetry $D(\xi)=D(-\xi)$. Consider now the $\hbar^n$ contributions $n=0,2,4$, of a prototype graph. Its classical value ($n=0$) is rapidly decreasing since all bonds are fast (this is in fact the standard classical Debye-Hückel theory). The $\hbar^2$ contribution results from the occurrence of one $\hbar^2$ bond or two $\hbar$ bonds, all other bonds being classical. In the first case, the $\hbar^2$ bond has necessarily classical ends and hence will be integrated on its ξ variables (since classical potential lines are independent of the ξ variables). Therefore the corresponding decay will be fast [see the remark after (4.30)]. In the second case the decay is also rapid since all $(\hbar,k)$ bonds are fast. We thus conclude that at the order $\hbar^2$ all graphs are rapidly decreasing. We now turn to the $\hbar^4$ contribution of a prototype graph; this contribution can result from the following situations.

(i) Four $\hbar$ bonds: this gives a rapid decay since all $\hbar$ bonds are fast.

(ii) Two $\hbar^2$ bonds: each of them must have at least one classical end, and so will be integrated on one of its ξ variables. This leads to a rapid decay.

(iii) One $\hbar$ bonds and one $\hbar^3$ bond: the decay is fast for the same reasons as in (i) and (ii).

(iv) One $\hbar^2$ bond and two $\hbar$ bonds: the only dangerous configuration of these bonds in the graph is that of Fig. 8 where the $\hbar$ bonds are attached to both extremities (i,j) of a $(\hbar^2,1)$ bond [remember that $\hbar$ bonds and $(\hbar^2,k)$ bonds, $k\geq 2$, are fast]. In all other configurations, the $(\hbar^2,1)$ bond has a classical end, hence giving a fast decay for the same reasons as in (ii). If the configuration of Fig. 8 occurs, we distinguish two cases.

(a) Suppose first that the graph is separated into two disjoint parts with root points $\mathbf{x}_1$ and $\mathbf{x}_2$ by removing the $(\hbar^2,1)$ bond. Then the value of the graph is necessarily of the form

$$\int d\mathbf{y}_i \int d\mathbf{y}_j \int D(\boldsymbol{\alpha}_i) \int D(\boldsymbol{\alpha}_j) G_1(\mathbf{x}_1-\mathbf{y}_i,\boldsymbol{\alpha}_i) \times \phi_1^{\mathrm{eff}(2)}(\mathbf{y}_i-\mathbf{y}_j,\boldsymbol{\alpha}_i,\boldsymbol{\alpha}_j) G_2(\mathbf{y}_j-\mathbf{x}_2,\boldsymbol{\alpha}_j) , \quad (4.33)$$

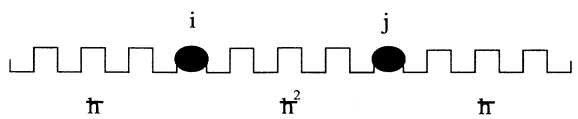

FIG. 8. Configuration with two $\hbar$ bonds attached to one $\hbar^2$ bond. Every $(\hbar^n,k)$ bond is represented by a crenelated line.

or, in Fourier representation,

$$\int D(\boldsymbol{\alpha}_i) \int D(\boldsymbol{\alpha}_j) G_1(\mathbf{k},\boldsymbol{\alpha}_i) \phi_1^{\mathrm{eff}(2)}(\mathbf{k},\boldsymbol{\alpha}_i,\boldsymbol{\alpha}_j) G_2(\mathbf{k},\boldsymbol{\alpha}_j) , \quad (4.34)$$

where G_1 and G_2 represent the total contributions of the parts of the graph attached to $(1,i)$ and $(j,2)$. Because of the rotational invariance of the $D(\boldsymbol{\alpha})$ measure, $G_a(\mathbf{k},\boldsymbol{\alpha})$ $(a=1,2)$ is invariant under the simultaneous rotations of the vectors $\mathbf{k}$ and $\boldsymbol{\alpha}$. Moreover G_a consists of classical bonds and one fast $\hbar$ bond, which is linear in $\boldsymbol{\alpha}$ [see (C22)]. This implies that G_a has to be of the form

$$G_a(\mathbf{k},\boldsymbol{\alpha}) = G_a(k^2)\mathbf{k}\cdot\left[\int_0^1 ds\, \boldsymbol{\alpha}(s)\right] , \quad (4.35)$$

where $G_a(k^2)$ is infinitely differentiable at $\mathbf{k}=\mathbf{0}$. Inserting (4.35) and the Fourier transform of (4.30) and (4.34), we see that the $\boldsymbol{\alpha}$ integration produces a k^2 factor, i.e.,

$$\int D(\boldsymbol{\alpha}) \left[\mathbf{k}\cdot\left[\int_0^1 ds\, \boldsymbol{\alpha}(s)\right]\right]^2 = \frac{1}{12}k^2 ,$$

which kills the Coulomb singularity of (4.30). Hence, (4.34) has no singularity at $\mathbf{k}=\mathbf{0}$ and the convolution (4.33) is rapidly decreasing.

(b) Assume now that the graph remains connected when the $(\hbar^2,1)$ bond is suppressed. Then the value of the graph is of the form

$$\int d\mathbf{y}_i \int d\mathbf{y}_j \int D(\boldsymbol{\alpha}_i) \int D(\boldsymbol{\alpha}_j) \times F(\mathbf{x}_1,\mathbf{x}_2;\mathbf{y}_i,\boldsymbol{\alpha}_i,\mathbf{y}_j,\boldsymbol{\alpha}_j) \phi_1^{\mathrm{eff}(2)}(\mathbf{y}_i-\mathbf{y}_j,\boldsymbol{\alpha}_i,\boldsymbol{\alpha}_j) , \quad (4.36)$$

where $F(\mathbf{x}_1,\mathbf{x}_2,;\mathbf{y}_i,\boldsymbol{\alpha}_i,\mathbf{y}_j,\boldsymbol{\alpha}_j)$ is the Mayer expression associated with a graph that is connected with respect to the root points $\mathbf{x}_1$, $\mathbf{x}_2$ and that is made of classical and $\hbar$ bonds. Since these bonds are fast, the value of the latter graph is rapidly decreasing as $|\mathbf{x}_1-\mathbf{x}_2|\to\infty$ and the same will be true for (4.36).

(v) It remains to examine the case where the graph has one $\hbar^4$ bond, the others being classical. The $(\hbar^4,k)$ bonds with $k\geq 3$ are fast and a $(\hbar^4,1)$ bond cannot lead to an algebraic decay since it has classical ends. Hence the only bonds susceptible of producing an algebraic decay are the $(\hbar^4,2)$ bonds coming from the insertion (4.17).

To analyze their effect, it is convenient to define the contribution $H(\mathbf{x}_1-\mathbf{x}_2,\xi_1,\xi_2)$ of the prototype graphs that remain connected when an insertion (4.17) is removed. Furthermore, we define

$$K(\mathbf{x}_1-\mathbf{x}_2,\xi_1,\xi_2) = H(\mathbf{x}_1-\mathbf{x}_2,\xi_1,\xi_2) + \rho(\mathbf{x}_1,\xi_1)\delta(\mathbf{x}_1-\mathbf{x}_2)\delta_{\xi_1,\xi_2} . \quad (4.37)$$

In (4.37), $\rho(\mathbf{x}_1,\xi_1)$ is the contribution of the set of

all graphs with one root point $(\mathbf{x}_1,\xi_1)$. By translation invariance $\rho(\mathbf{x}_1,\xi_1)$ is independent of $\mathbf{x}_1$ and $\int D(\xi_1)\rho(\mathbf{x}_1,\xi_1)=\rho$ is the electronic density. Then one can write for

$$S(\mathbf{x}_1-\mathbf{x}_2)=\rho_T(\mathbf{x}_1-\mathbf{x}_2)+\rho\delta(\mathbf{x}_1-\mathbf{x}_2)$$

an exact Dyson equation, which reads in Fourier representation

$$S(\mathbf{k})=\int D(\xi_1)\int D(\xi_2)\left[K(\mathbf{k},\xi_1,\xi_2)+\sum_{N=1}^{\infty}\int D(\alpha_1)\cdots D(\alpha_N)D(\alpha_1')\cdots D(\alpha_N')\times K(\mathbf{k},\xi_1,\alpha_1)V_2(\mathbf{k},\alpha_1,\alpha_1')K(\mathbf{k},\alpha_1',\alpha_2)\cdots V_2(\mathbf{k},\alpha_N,\alpha_N')K(\mathbf{k},\alpha_N',\xi_2)\right]. \quad (4.38)$$

As shown before, the algebraic decay of ρ_T at the order $\hbar^4$ can only result from the occurrence of one $(\hbar^4,2)$ bond, all other bonds being classical. If such a graph remains connected by removing this $(\hbar^4,2)$ bond, the decay will be rapid according to the same argument as that given in (iv b). Hence, in view of the definition of H, the algebraic decay of ρ_T is due to the $(\hbar^4,2)$ bond appearing in the V_2 functions in (4.38). Thus $\rho_T^{(4)\mathrm{alg}}(\mathbf{k})$, the dominant nonanalytic part of a $\rho_T(\mathbf{k})$ at the order $\hbar^4$, is obtained by making all functions classical in (4.38) except one of the V_2 factors. The dominant nonanalytic part of a V_2 term, after integration of the ξ variables of its end points, has already been calculated in (4.22) and (4.25). Performing these operations in (4.38), one finds

$$\begin{aligned}\hbar^4\rho_T^{\mathrm{alg}(4)}(\mathbf{k})&=V_2^{\mathrm{alg}(4)}(\mathbf{k})\sum_{n=1}^{\infty}n[V_2^{\mathrm{cl}}(\mathbf{k})]^{n-1}[K^{\mathrm{cl}}(\mathbf{k})]^{n+1}\\&=V_2^{\mathrm{alg}(4)}(\mathbf{k})\left[\frac{K^{\mathrm{cl}}(\mathbf{k})}{1-V_2^{\mathrm{cl}}(\mathbf{k})K^{\mathrm{cl}}(\mathbf{k})}\right]^2\\&=V_2^{\mathrm{alg}(4)}(\mathbf{k})[S^{\mathrm{cl}}(\mathbf{k})]^2\ . \quad (4.39)\end{aligned}$$

In (4.39), V_2^{cl} and K^{cl} are the classical limits of (4.17) and (4.37) and

$$\begin{aligned}S^{\mathrm{cl}}(\mathbf{k})&=K^{\mathrm{cl}}(\mathbf{k})+K^{\mathrm{cl}}(\mathbf{k})\sum_{n=1}^{\infty}[V_2^{\mathrm{cl}}(\mathbf{k})K^{\mathrm{cl}}(\mathbf{k})]^n\\&=\frac{K^{\mathrm{cl}}(\mathbf{k})}{1-V_2^{\mathrm{cl}}(\mathbf{k})K^{\mathrm{cl}}(\mathbf{k})} \quad (4.40)\end{aligned}$$

is the classical structure factor of the one-component plasma, represented by the classical analog of the Dyson equation (4.38). Finally, inserting (4.22) with (4.25) into (4.39), as well as the small-$\mathbf{k}$ behavior of $S^{\mathrm{cl}}(\mathbf{k})$ (the Stillinger-Lovett sum rule [10])

$$\lim_{|\mathbf{k}|\to 0}S^{\mathrm{cl}}(\mathbf{k})\approx\frac{1}{4\pi\beta e^2}|\mathbf{k}|^2 \quad (4.41)$$

one obtains

$$\hbar^4\rho_T^{(4)\mathrm{alg}}(\mathbf{k})=\frac{1}{(8)(4!)240}\hbar^4\left[\frac{\beta}{m}\right]^2|\mathbf{k}|^7\ . \quad (4.42)$$

Since the inverse Fourier transform of $|\mathbf{k}|^7$ is $(8!/2\pi^2)1/|\mathbf{x}|^{10}$, (4.42) corresponds to the following spatial decay of the structure function:

$$\lim_{|\mathbf{x}|\to\infty}S^{(4)}(\mathbf{x})\approx\frac{7}{16\pi^2}\left[\frac{\beta}{m}\right]^2\frac{1}{|\mathbf{x}|^{10}}\ , \quad (4.43)$$

which has been found in Ref. [1] by different methods.

It is worth noting that in (4.39) the screening properties expressed by the classical Stillinger-Lovett sum rule (4.41) modifies the $1/|\mathbf{x}|^6$ decay of the squared dipolar effective potential (4.19) to $1/|\mathbf{x}|^{10}$ for the full charge-charge correlation function. This was already pointed out in Ref. [1]. Similarly, in Sec. III B, the same change from $1/|\mathbf{x}|^6$ for $U^{\mathrm{eff}}(\mathbf{x},n=0)$ to $1/|\mathbf{x}|^{10}$ for $S(\mathbf{x},n=0)$ was due to the quantum sum rule (2.15) together with the resummations implied by the Dyson equation (2.11).

Moreover, in our quantum Mayer bonds formalism, it is easily seen that the analog of the ladder diagram of order $N\geq 3$ introduced in Sec. III B involves the Nth power of the dipolar effective potential and so leads to a faster decay than the diagram of Fig. 7.

V. CONCLUDING REMARKS

In this paper, we have given another evidence that there is no exponential screening in the quantum electron gas at thermal equilibrium. This evidence relies on the existence of graphs in the many-body perturbative expansion that do not decay exponentially fast at large distances. Equivalently, the frequency components $U^{\mathrm{eff}}(\mathbf{k},n)$ of the effective potential and the frequency components $S(\mathbf{k},n)$ of the structure function as well as the inverse dielectric function $1/\epsilon(\mathbf{k})$ are not analytic at $\mathbf{k}=0$. Although we did not control the full diagrammatic development, we give plausible arguments that $U^{\mathrm{eff}}(\mathbf{k},n=0)$, $S(\mathbf{k},n)$ and $1/\epsilon(\mathbf{k})$ have, respectively, a $|\mathbf{k}|^3$, $|\mathbf{k}|^7$, and $|\mathbf{k}|^5$ term in their small-$\mathbf{k}$ expansion corresponding to $1/|\mathbf{x}|^6$, $1/|\mathbf{x}|^{10}$, and $1/|\mathbf{x}|^8$ spatial decay. We note that the decay of $S(\mathbf{x})$ obtained here from perturbation theory is faster than $1/|\mathbf{x}|^6$ in agreement with the constraints imposed by the exact hierarchy equations for the imaginary time Green's functions [1]. We also see that the introduction of the Fermi statistics, at least as far as the graph of Fig. 3 and the whole class of ladder diagrams (see Fig. 4) are concerned, does not modify quali-

tatively the semiclassical result (1.2).

As shown in Sec. III A, $S_{\mathrm{RPA}}(\mathbf{x})$ satisfies the sum rule (2.15) with respect to the density of the free gas. This is no more the case when the single additional graph Π_1^* of Fig. 3 is taken into account. In fact, the validity of (2.15) requires $A_0(n)=0$ for $n\neq 0$ [see (2.26)], but it can be checked that the contribution of Π_1^* to $A_0(n)$ does not vanish. It is an open question to find a consistent model of $S(\mathbf{x})$ that simultaneously satisfies the basic screening sum rules together with the correct algebraic asymptotic behavior.

The conclusions of Secs. II and III hold under the additional assumption that the functions have no other singularities for real values of the components of $\mathbf{k}$ different from zero when the temperature is strictly positive. The situation is drastically different at zero temperature because of the sharpness of the Fermi surface in perturbation theory. Already the structure factor of the free Fermi gas in its ground state has a $|\mathbf{k}|$ term due to the exchange term [11]. This causes a decay as slow as $1/|\mathbf{x}|^4$. Moreover, the effective potential in the zero-temperature RPA treatment of the Coulomb gas shows the long-range Friedel oscillations $\cos(2k_F|\mathbf{x}|)/|\mathbf{x}|^3$, where k_F is the Fermi wave number. The absence of exponential screening will still be reflected by the occurrence of algebraically decaying terms of higher order, but this will be completely hidden at large distances by the longer tails linked to the nonsmooth effects of the Fermi statistics. The study at low temperature of the crossover regime between these two types of behaviors (i.e., between algebraiclike decays due either to Fermi statistics or to Coulombic screening) would be interesting.

We emphasize once more that the lack of exponential screening has a quantum-mechanical origin which is mostly clearly exhibited in the semiclassical treatment of Sec. IV. As shown by the functional integration formalism, because of their intrinsic quantum fluctuations, point quantum particles behave effectively as extended random-charge distributions capable of multipolar interactions. Moreover, the quantum potential (4.2) is not identical to the classical electrostatic pair potential between two charged wires which would be of the form

$$\phi^{\mathrm{classical}}(\mathbf{x}_1-\mathbf{x}_2,\xi_1,\xi_2)=\int_0^1 ds_1\int_0^1 ds_2\,U_0(\mathbf{x}_1-\mathbf{x}_2+\lambda\xi_1(s_1)-\lambda\xi_2(\mathbf{s}_2))\ . \tag{5.1}$$

According to (C5) and since

$$\int_0^1 ds_1\int_0^1 ds_2\,\tilde{\Pi}_0(\mathbf{k},s_1-s_2)=\tilde{\Pi}_0(\mathbf{k},n=0)\ ,$$

it is easily verified that the effective chain potential corresponding to (5.1) is given by

$$\phi_{\mathrm{chain}}^{\mathrm{classical}}(\mathbf{k},\xi_1,\xi_2)=U_0(\mathbf{k})\left[1+\sum_{N=1}^{\infty}[U_0(\mathbf{k})\tilde{\Pi}_0(\mathbf{k},n=0)]^N\right]\int_0^1 ds_1\int_0^1 ds_2 e^{i\lambda\mathbf{k}\cdot[\xi_1(s_1)-\xi_2(s_2)]}$$
$$=\frac{4\pi\beta e^2}{k^2-4\pi\beta e^2\tilde{\rho}_0\tilde{\Pi}_0(\mathbf{k},n=0)}\int_0^1 ds_1\int_0^1 ds_2 e^{i\lambda\mathbf{k}\cdot[\xi_1(s_1)-\xi_2(s_2)]}\ . \tag{5.2}$$

Clearly (5.2) is of Debye-Hückel type as $|\mathbf{k}|\to 0$ and the truly classical system defined by (5.1) has the property of exponential screening. The quantum potential (4.2) differs essentially from (5.1) by the fact that it involves only "equal time" contributions. Thus, the nonexponential screening discussed in this paper is a pure quantum-mechanical effect with no classical analog.

Note added. After the completion of this work, N. W. Ashcroft kindly informed us of two papers [A. C. Maggs and N. W. Ashcroft, Phys. Rev. Lett. **59**, 113 (1987); D. C. Langreth and S. H. Vosko, *ibid.* **59**, 497 (1987)], in which the diagram of Fig. 3 is considered and shown to have a $1/|\mathbf{x}|^6$ decay for the electron gas at zero temperature.

ACKNOWLEDGMENTS

We acknowledge the Laboratoire de Physique Théorique et Hautes Energies associé au Centre National de la Recherche Scientifique. One of us (F.C.) thanks the Institut de Physique Théorique of the Ecole Polytechnique Fédérale de Lausanne for its kind hospitality. The work was partially supported by the Swiss National Foundation for Science.

APPENDIX A

In this appendix we retrieve the small-$\mathbf{k}$ expansion of $\Pi_0(k,n)$ at the order k^2 by methods that will also be used in Appendix B.

The Fourier transform of $\Pi_0(k,s)$ defined in (3.1) reads

$$\Pi_0(\mathbf{k},n)\equiv\Pi_0(\mathbf{k},\omega_{2n})$$
$$=2\int\frac{d\mathbf{p}}{(2\pi)^3}\sum_{m=-\infty}^{+\infty}G_0(\mathbf{p}+\mathbf{k},m+n)G_0(\mathbf{p},m)$$
$$=2\int\frac{d\mathbf{p}}{(2\pi)^3}\sum_{m=-\infty}^{+\infty}G_0(\mathbf{p}+\mathbf{k},m)G_0(\mathbf{p},m-n)\ , \tag{A1}$$

where $G_0(\mathbf{p},m)$ is the s-Fourier transform of (3.2), defined as in (2.7),

$$G_0(\mathbf{p},m)\equiv G_0(\mathbf{p},\omega_{2m+1})=\frac{1}{i\pi(2m+1)-(\lambda^2p^2/2-\beta\mu)}\ . \tag{A2}$$

According to the definition (3.1) $\Pi_0(\mathbf{x},s)=\Pi_0(\mathbf{x},-s)$, and therefore $\Pi_0(\mathbf{k},n)=\Pi_0(\mathbf{k},-n)$. In order to preserve this parity property through the small-$\mathbf{k}$ expansion of

$\Pi_0(\mathbf{k},n)$, we rather consider the following expression:

$$\Pi_0(\mathbf{k},n) = 2\int \frac{d\mathbf{p}}{(2\pi)^3} EP_n \left[\sum_{m=-\infty}^{+\infty} G_0(\mathbf{p}+\mathbf{k},m) G_0(\mathbf{p},m+n) \right], \tag{A3}$$

where $EP_n[f(m,n)]$ denotes the part of $f(m,n)$ which is even in n:

$$EP_n[f(m,n)] \equiv [f(m,n)+f(m,-n)]/2 .$$

According to (A2) the small-$\mathbf{k}$ expansion of $G_0(\mathbf{p}+\mathbf{k},m)$ is very simple:

$$G_0(\mathbf{p}+\mathbf{k},m) = \sum_{j=0}^{+\infty} v_{\mathbf{k}}^j(p)[G_0(p,m)]^{j+1} \tag{A4}$$

with

$$v_{\mathbf{k}}(p) \equiv \frac{\lambda^2}{2}[(\mathbf{p}+\mathbf{k})^2-\mathbf{p}^2] = \lambda^2(\mathbf{p}\cdot\mathbf{k}+\tfrac{1}{2}k^2)$$

Because of the rotational invariance of $G_0(p,m)$ we can use the identities

$$\int d\mathbf{p} v_{\mathbf{k}}(\mathbf{p}) f(|\mathbf{p}|) = \frac{\lambda^2 k^2}{2}\int d\mathbf{p} f(|\mathbf{p}|) ,$$
$$\int d\mathbf{p} v_{\mathbf{k}}^2(\mathbf{p}) f|\mathbf{p}|) = \lambda^2 k^2 \int d\mathbf{p} \frac{\lambda^2 p^2}{3} f(|\mathbf{p}|) + O(k^4) , \tag{A5}$$

and we obtain in this way

$$\Pi_0(\mathbf{k},n) = 2\int \frac{d\mathbf{p}}{(2\pi)^3} EP_n \left[P_2(p;n) + \frac{\lambda^2 k^2}{2} P_3(p;n) + \lambda^2 k^2 \frac{\lambda^2 p^2}{3} P_4(p;n) \right] + O(k^4) \tag{A6}$$

with

$$P_N(p;n) \equiv \sum_{m=-\infty}^{+\infty} \{[G_0(p,m)]^{N-1} G_0(p,m+n)\} . \tag{A7}$$

To evaluate $P_N(p;n)$ we first decompose the products of G_0's into sums of simple fractions by using

$$G_0(p,m)G_0(p,m+n) = \frac{1}{2i\pi n}[G_0(p,m)-G_0(p,m+n)] , \quad \text{if } n\neq 0 . \tag{A8}$$

This leads to

$$P_2(p;n) = \delta_{n,0}\gamma_2(p) ,$$
$$P_3(p;n) = \delta_{n,0}\gamma_3(p) + (1-\delta_{n,0})\frac{1}{2i\pi n}\gamma_2(p) , \tag{A9}$$
$$P_4(p;n) = \delta_{n,0}\gamma_4(p) + (1-\delta_{n,0})\left[\frac{1}{2i\pi n}\gamma_3(p) + \frac{1}{4\pi^2 n^2}\gamma_2(p)\right] ,$$

with $\gamma_N(p) \equiv P_N(p;n=0)$. The expression (3.7) of $\gamma_N(p)$ follows from the usual method of calculating frequency sums by contour integration (see Ref. [4], Sec. 25) and the remark that

$$\left[\frac{1}{i\pi(2m+1)-\zeta}\right]^N = \frac{1}{(N-1)!}\frac{d^{N-1}}{d\zeta^{N-1}}\left[\frac{1}{i\pi(2m+1)-\zeta}\right] . \tag{A10}$$

For instance

$$\gamma_1(p) = n_0(p) ,$$
$$\gamma_2(p) = -n_0(p)[1-n_0(p)] ,$$
$$\gamma_3(p) = \tfrac{1}{2}n_0(p)[1-n_0(p)][1-2n_0(p)] , \tag{A11}$$
$$\gamma_4(p) = -\tfrac{1}{6}n_0(p)][1-n_0(p)]\{1-6n_0(p)+6[n_0(p)]^2\} .$$

An integration by parts combined with (A10) leads to

$$\int d\mathbf{p} \frac{\lambda^2 p^2}{3}\gamma_N(p) = -\frac{1}{N-1}\int d\mathbf{p}\gamma_{N-1}(p) . \tag{A12}$$

Finally, by using (A9) and (A12) and retaining only the even parts in n of $P_N(p;n)$ in (A6), we obtain (3.5).

APPENDIX B

In this appendix, we study the small $\mathbf{q}_1,\mathbf{q}_2$ expansion of $\Lambda_0^{\text{alg}}(\mathbf{q}_1,\mathbf{q}_2,n_1,n_2)$, defined in (3.18), to second order in $\mathbf{q}_1\cdot\mathbf{q}_2$ and we derive a useful property of $\Lambda_0(\mathbf{q}_1,\ldots,\mathbf{q}_N,n_1,\ldots,n_N)$ defined in (3.27).

In order to deal with $\Lambda_0^{\text{alg}}(\mathbf{q}_1,\mathbf{q}_2,n_1,n_2)$ we first check the property (3.15) by translating the dummy variables m to $m-n_1-n_2$ and $\mathbf{p}$ to $\mathbf{p}-\mathbf{q}_1-\mathbf{q}_2$ in (3.14), then changing $\mathbf{p}$ into $-\mathbf{p}$ and using $G_0(-\mathbf{p},m)=G_0(\mathbf{p},m)$. As in Appendix A, order to preserve the parity property (3.15) through the small $\mathbf{q}_1,\mathbf{q}_2$ expansion of $\Lambda_0(\mathbf{q}_1,\mathbf{q}_2,n_1,n_2)$, we rewrite the latter as

$$\Lambda_0(\mathbf{q}_1,\mathbf{q}_2,n_1,n_2) = \int \frac{d\mathbf{p}}{(2\pi)^3} EP_{n_1,n_2}\left[\sum_{m=-\infty}^{+\infty} [G_0(\mathbf{p},m)G_0(\mathbf{p}+\mathbf{q}_1,m+n_1)G_0(\mathbf{p}+\mathbf{q}_1+\mathbf{q}_2,m+n_1+n_2) G_0(\mathbf{p},m)G_0(\mathbf{p}+\mathbf{q}_2,m+n_2)G_0(\mathbf{p}+\mathbf{q}_1+\mathbf{q}_1,m+n_1+n_2)]\right] , \tag{B1}$$

where $EP_{n_1,n_2}[f(m,n_1,n_2)]$ denotes the part of $f(m,n_1,n_2)$ which is simultaneously even in n_1 and n_2:

$$EP_{n_1,n_2}[f(m,n_1,n_2)] \equiv \tfrac{1}{2}[f(m,n_1,n_2)+f(m,-n_1,-n_2)] .$$

Moreover, in order to simplify the subsequent expansions of $\mathbf{q}_1$ and $\mathbf{q}_2$, we translate the dummy variable $\mathbf{p}$ to $\mathbf{p}-\mathbf{q}_1$ (to $\mathbf{p}-\mathbf{q}_2$) in the first (second) sum of (B1) and rewrite the latter as

$$\Lambda_0(\mathbf{q}_1,\mathbf{q}_2,n_1,n_2)=\int\frac{d\mathbf{p}}{(2\pi)^3}EP_{n_1,n_2}\left[\sum_{m=-\infty}^{+\infty}[G_0(\mathbf{p}-\mathbf{q}_1,m)G_0(\mathbf{p},m+n_1)G_0(\mathbf{p}+\mathbf{q}_2,m+n_1+n_2)\right.$$
$$\left.+G_0(\mathbf{p}-\mathbf{q}_2,m)G_0(\mathbf{p},m+n_2)G_0(\mathbf{p}+\mathbf{q}_1,m+n_1+n_2)]\right]. \tag{B2}$$

After expanding the propagators G_0's in small $\mathbf{q}_1$ and $\mathbf{q}_2$ according to (A4), we find that the only terms in $\Lambda_0(\mathbf{q}_1,\mathbf{q}_2,n_1,n_2)$ which are proportional either to a constant, to $\mathbf{q}_1\cdot\mathbf{q}$ or to $(\mathbf{q}_1\cdot\mathbf{q}_2)^2$ result from the following equalities for a spherically symmetrical function $f(|\mathbf{p}|)$:

$$\int d\mathbf{p}\,v_{-\mathbf{q}_1}v_{\mathbf{q}_2}f(|\mathbf{p}|)=-\lambda^2\mathbf{q}_1\cdot\mathbf{q}_2\int d\mathbf{p}\frac{\lambda^2p^2}{3}f(|\mathbf{p}|)+\lambda^4\tfrac{1}{4}q_1^2q_2^2\int d\mathbf{p}\,f(|\mathbf{p}|)\,,$$
$$\int d\mathbf{p}(v_{-\mathbf{q}_1})^2(v_{\mathbf{q}_2})^2f(|\mathbf{p}|)=\lambda^4\tfrac{2}{3}(\mathbf{q}_1\cdot\mathbf{q}_2)^2\int d\mathbf{p}\frac{\lambda^4p^4}{5}f(|\mathbf{p}|)+\lambda^4\tfrac{1}{3}q_1^2q_2^2\int d\mathbf{p}\frac{\lambda^4p^4}{5}f(|\mathbf{p}|)+o(q_1^2q_2^2)\,. \tag{B3}$$

After some translations of the dummy summation variable m in (B2) and collecting identical series, we obtain

$$\Lambda_0^{\mathrm{alg}}(\mathbf{q}_1,\mathbf{q}_2,\nu,n-\nu)=2\int\frac{d\mathbf{p}}{(2\pi)^3}EP_{\nu,n}\left[L_3(p;n,\nu)-\lambda^2\mathbf{q}_1\cdot\mathbf{q}_2\frac{\lambda^2p^2}{3}L_5(p;n,\nu)+\lambda^4(\mathbf{q}_1\cdot\mathbf{q}_2)^2\frac{2}{3}\frac{\lambda^4p^4}{5}L_7(p;n,\nu)\right], \tag{B4}$$

with

$$L_{2N+1}(p;n,\nu)\equiv\sum_{m=-\infty}^{+\infty}\{[G_0(p,m)]^NG_0(p,m+\nu)[G_0(p,m+n)]^N\}\,. \tag{B5}$$

Decomposing again products of G_0's into sums, we obtain in the same way as in Appendix A

$$EP_{\nu,n}[L_3(p;n,\nu)]=\delta_{n,0}\delta_{\nu,0}\gamma_3(p)\,,$$
$$EP_{\nu,n}[L_5(p;n,\nu)]=\delta_{n,0}\left[\delta_{\nu,0}\gamma_5(p)+(1-\delta_{\nu,0})\frac{\gamma_3(p)}{4\pi^2\nu^2}\right]-\frac{(1-\delta_{n,0})}{4\pi^2n^2}(\delta_{\nu,0}+\delta_{\nu,n})\gamma_3(p) \tag{B6}$$
$$EP_{\nu,n}[L_7(p;n,\nu)]=\delta_{n,0}\left[\delta_{\nu,0}\gamma_7(p)+(1-\delta_{\nu,0})\left[\frac{\gamma_5(p)}{4\pi^2\nu^2}-\frac{\gamma_3(p)}{(4\pi^2\nu^2)^2}\right]\right]$$
$$-\frac{(1-\delta_{n,0})}{4\pi^2n^2}\left[-(\delta_{\nu,0}+\delta_{\nu,n}\frac{3}{4\pi^2n^2}+(1-\delta_{\nu,0})\frac{1}{4\pi^2n\nu}+(1-\delta_{\nu,n})\frac{1}{4\pi^2n(n-\nu)}\right]\gamma_3(p)\,,$$

with the $\gamma_N(p)$'s defined in (A9). By using the relation (A12) for $N=3$ and 5 and the similar relation

$$\int d\mathbf{p}\frac{\lambda^4p^4}{5}\gamma_N(p)=\frac{3}{(N-1)(N-2)}\int d\mathbf{p}\gamma_{N-2}(p) \tag{B7}$$

for $N=3,5,7$ a straightforward calculation leads to

$$\Lambda_0^{\mathrm{alg}}(\mathbf{q}_1,\mathbf{q}_2,\nu,n-\nu)=\delta_{n,0}\delta_{\nu,0}2\Gamma_3+\lambda^2\mathbf{q}_1\cdot\mathbf{q}_2\left[\delta_{n,0}\left[\delta_{\nu,0}\frac{\Gamma_4}{2}+(1-\delta_{\nu,0})\frac{\Gamma_2}{4\pi^2\nu^2}\right]-\frac{(1-\delta_{n,0})}{4\pi^2n^2}(\delta_{\nu,0}+\delta_{\nu,n})\frac{\Gamma_2}{4\pi^2n^2}\right]$$
$$+\lambda^4(\mathbf{q}\cdot\mathbf{q}_2)^2\left\{\delta_{n,0}\left[\delta_{\nu,0}\frac{2\Gamma_5}{15}+(1-\delta_{\nu,0})\left[\frac{\Gamma_3/3}{4\pi^2\nu^2}-\frac{2\Gamma_1}{(4\pi^2\nu^2)^2}\right]\right]\right.$$
$$\left.+\frac{(1-\delta_{n,0})}{4\pi^2n^2}\left[-(\delta_{\nu,0}+\delta_{\nu,n})\frac{6\Gamma_1}{4\pi^2n^2}+(1-\delta_{\nu,0})\frac{2\Gamma_1}{4\pi^2n\nu}+(1-\delta_{\nu,n})\frac{2\Gamma_1}{4\pi^2n(n-\nu)}\right]\right\}. \tag{B8}$$

We now prove the property (3.28) of $\Lambda_0^{\mathrm{alg}}(\mathbf{q}_1,\ldots,\mathbf{q}_N,n_1,\ldots,n_N)$. According to the symmetries exhibited by the definition (3.27), the small $\mathbf{q}_i$'s expansion of $\Lambda_0(\mathbf{q}_1,\ldots,\mathbf{q}_N,n_1,\ldots,n_N)$ to second order in the $\mathbf{q}_i$'s has the following form:

$$\Lambda_0(\mathbf{q}_1,\ldots,\mathbf{q}_N,n_1,\ldots,n_N)=\lambda_0(n_1,\ldots,n_N)+\sum_{i\neq j}\lambda_1(n_i,n_j|\{n_k\}_{k\neq i,j})\mathbf{q}_i\cdot\mathbf{q}_j+\sum_i\mu_1(n_i|\{n_k\}_{k\neq i})|\mathbf{q}|^2\cdots\,, \tag{B9}$$

where the ellipsis represents terms of fourth order in the $\mathbf{q}_i$'s and where $\lambda_0(n_1,\ldots,n_N)$ [$\lambda_1(n_i,n_j|\{n_k\}_{k\neq i,j})$ and $\mu_1(n_i|\{n_k\}_{k\neq 1})$] is symmetrical under any permutation of $n_1,\ldots,n_N$ (of the n_k's). Moreover

$$\lambda_1(n_i,n_j|\{n_k\}_{k\neq i,j})=\lambda_1(n_j,n_i|\{n_k\}_{k\neq i,j}) .$$

Thus, when studying the properties of $\Lambda_0(\mathbf{q}_1,\ldots,\mathbf{q}_N,n_1,\ldots,n_N)$ at the second order in the $\mathbf{q}_i$'s, it is sufficient to consider $\Lambda_0(\mathbf{q}_1=\mathbf{0},\mathbf{q}_2,\ldots,\mathbf{q}_N,n_1,\ldots,n_N)$. We rewrite (3.27) with $\mathbf{q}_i=\mathbf{0}$ as

$$\begin{aligned}\Lambda_0(\mathbf{q}_1=\mathbf{0},\mathbf{q}_2,\ldots,\mathbf{q}_N,n_1,\ldots,n_N)=\int\frac{d\mathbf{p}}{(2\pi)^3}\sum_{\pi\in\Pi_{N-1}}\Big[&G_0(\mathbf{p},m)G_0(\mathbf{p},m+n_1)G_0(\mathbf{p}+\mathbf{q}_{\pi_2},m+n_1+n_{\pi_2})\\&\times\cdots\times G_0(\mathbf{p}+\mathbf{q}_{\pi_2}+\cdots+\mathbf{q}_{\pi_N},m+n_1+n_{\pi_2}+\cdots\ n_{\pi_N})\\&+\sum_{k=2}^{N-1}G_0(\mathbf{p},m)G_0(\mathbf{p}+\mathbf{q}_{\pi_2},m+n_{\pi_2})\\&\quad\times\cdots\times G_0(\mathbf{p}+\mathbf{q}_{\pi_2}+\cdots+\mathbf{q}_{\pi_k},m+n_{\pi_2}+\cdots+n_{\pi_k})\\&\quad\times G_0(\mathbf{p}+\mathbf{q}_{\pi_2}+\cdots+\mathbf{q}_{\pi_k},m+n_1+n_{\pi_2}+\cdots+n_{\pi_k})\\&\quad\times G_0(\mathbf{p}+\mathbf{q}_{\pi_2}+\cdots+\mathbf{q}_{\pi_{k+1}},m+n_1+n_{\pi_2}+\cdots+n_{\pi_{k+1}})\\&\quad\times\cdots\times G_0(\mathbf{p}+\mathbf{q}_{\pi_2}+\cdots+\mathbf{q}_{\pi_N},m+n_1+n_{\pi_2}+\cdots+n_{\pi_N})\\&+G_0(\mathbf{p},m)G_0(\mathbf{p}+\mathbf{q}_{\pi_2},m+n_{\pi_2})\\&\quad\times\cdots\times G_0(\mathbf{p}+\mathbf{q}_{\pi_2}+\cdots+\mathbf{q}_{\pi_N},m+n_{\pi_2}+\cdots+n_{\pi_N})\\&\quad\times G_0(\mathbf{p}+\mathbf{q}_{\pi_2}+\cdots+\mathbf{q}_{\pi_N},m+n_1+n_{\pi_2}+\cdots+n_{\pi_N})\Big] ,\end{aligned}\tag{B10}$$

where Π_{N-1} denotes the group of the permutations of $\{2,\ldots,N\}$.

Assuming now that $n_1\neq 0$, we can use the relation (A8) for each product

$$G_0(\mathbf{p}+\mathbf{q}_{\pi_2}+\cdots+\mathbf{q}_{\pi_k},m+n_{\pi_2}+\cdots+n_{\pi_k})G_0(\mathbf{p}+\mathbf{q}_{\pi_2}+\cdots+\mathbf{q}_{\pi_k},m+n_1+n_{\pi_2}+\cdots+n_{\pi_k})$$

occurring in (B10) and rewrite the summation over k as a difference. Then changing the dummy variable m to $m-n_1$ in the term involving the product

$$G_0(\mathbf{p},m+n_1)G_0(\mathbf{p}+\mathbf{q}_{\pi_2},m+n_1+n_{\pi_2})\cdots G_0(\mathbf{p}+\mathbf{q}_{\pi_2}+\cdots+\mathbf{q}_{\pi_N},m+n_1+n_{\pi_2}+\cdots+n_{\pi_N}) ,$$

we see an exact cancellation of all the terms. Thus we find that

$$\Lambda_0(\mathbf{q}_1=\mathbf{0},\mathbf{q}_2,\ldots,\mathbf{q}_N,n_1,\ldots,n_N)=0 \quad \text{if } n_1\neq 0 .\tag{B11}$$

Hence the symmetrical coefficients in (B9) necessarily have the following structure:

$$\lambda_0(n_1,\ldots,n_N)=\lambda_0\delta_{n_1,0}\cdots\delta_{n_N,0} \quad \text{if } N\geq 2$$

and

$$\lambda_1(n_i,n_j|\{n_k\}_{k\neq i,j})=\lambda_1(n_1,n_i)\prod_{k\neq i,j}\delta_{n_k,0} \quad \text{if } N\geq 3 .\tag{B12}$$

APPENDIX C

In this appendix we show how the effective chain potential (4.9) introduced in the Boltzmann statistics regime is related to the RPA effective potential (3.4) and we study some of its properties.

In Fourier representation, the effective potential (4.9) reads

$$\phi^{\text{eff}}(\mathbf{k},\xi_1,\xi_2)=\phi(\mathbf{k},\xi_1,\xi_2)+\sum_{N=1}^{\infty}(-2z)^N\int D(\alpha_1)\cdots D(\alpha_N)\phi(\mathbf{k},\xi_1,\alpha_1)\phi(\mathbf{k},\alpha_1,\alpha_2)\cdots\phi(\mathbf{k},\alpha_N,\xi_2) ,\tag{C1}$$

where $\phi(\mathbf{k},\xi_1,\xi_2)$ is the $\mathbf{k}$ Fourier transform of (4.2).

$$\phi(\mathbf{k},\xi_1,\mathbf{x}_2)=U_0(\mathbf{k})\int_0^1 ds\, e^{-i\lambda\mathbf{k}\cdot[\xi_1(s)-\xi_2(s)]} ,\tag{C2}$$

with $U_0(\mathbf{k})$ given by (2.12). Hence, one finds

$$\phi^{\text{eff}}(\mathbf{k},\xi_1,\xi_2)=\int_0^1 ds_1 \int_0^1 ds_2 e^{-i\lambda\mathbf{k}\cdot[\xi_1(s_1)-\xi_2(s_2)]}\phi^{\text{eff}}(\mathbf{k},s_1-s_2)\ , \tag{C3}$$

where

$$\phi^{\text{eff}}(\mathbf{k},s_1-s_2)=U_0(\mathbf{k})\left[\delta(s_1-s_2)+U_0(\mathbf{k})\tilde{\Pi}_0(\mathbf{k},s_1-s_2)\right.$$
$$\left.+\sum_{N=2}^{\infty}[U_0(\mathbf{k})]^N\int_0^1 d\sigma_1\cdots\int_0^1 d\sigma_{N-1}\tilde{\Pi}_0(\mathbf{k},s_1-\sigma_1)\tilde{\Pi}_0(\mathbf{k},\sigma_1-\sigma_2)\cdots\tilde{\Pi}_0(\mathbf{k},\sigma_{N-1}-s_2)\right]\ , \tag{C4}$$

In (C4) we have introduced $\tilde{\Pi}_0(\mathbf{k},s_1-s_2)$ which is defined as the limit of $\Pi_0(\mathbf{k},s_1-s_2)$ in the Boltzmann statistics regime (where $\lambda^2k^2/2\gg\beta\mu$), and we have made the identification

$$\tilde{\Pi}_0(\mathbf{k},s_1-s_2)=-\tilde{\rho}_0\int D(\boldsymbol{\alpha})e^{i\lambda\mathbf{k}\cdot[\alpha(s_1)-\alpha(s_2)]} \tag{C5}$$

where $\tilde{\rho}_0=2z=2e^{\beta u}/(2\pi\lambda^2)^{3/2}$ is the density of a classical noninteracting gas with two internal degrees of freedom, with chemical potential μ and Boltzmann statistics. Indeed, when the Fermi statistics is suppressed, the free propagator (3.2) becomes

$$\tilde{G}_0(p,s)=-\theta(s)e^{-(\lambda^2p^2/2-\beta\mu)s}+\theta(-s)e^{-(\lambda^2p^2/2-\beta\mu)(s+1)} \tag{C6}$$

and therefore, according to (3.1), the free polarization insertion tends to

$$\tilde{\Pi}_0(\mathbf{k},s)=-\tilde{\rho}_0e^{-(\lambda^2k^2/2)|s|(1-|s|)} \tag{C7}$$

[note that we also have $\tilde{\rho}_0=\lim_{s\to0^-}2\tilde{G}_0(\mathbf{x}=\mathbf{0},s)$]. On the other hand, since the measure $D(\boldsymbol{\alpha})$ is Gaussian, one finds easily with the help of (4.1) that

$$\int D(\boldsymbol{\alpha})e^{i\lambda\cdot[\alpha(s_1)-\alpha(s_2)]}=e^{-(\lambda^2/2)\langle\{\mathbf{k}\cdot[\alpha(s_1)-\alpha(s_2)]\}^2\rangle}=e^{-(\lambda^2k^2/2)|s_1-s_2|(1-|s_1-s_2|)} \tag{C8}$$

Comparing (C7) with (C8) leads to the identification (C5).

Since $\tilde{\Pi}_0(k,s)$ is periodic with period 1, like $\Pi_0(k,s)$, it can be represented by the Fourier series

$$\tilde{\Pi}_0(k,s)=\sum_{n=-\infty}^{\infty}\tilde{\Pi}_0(k,n)e^{-2i\pi ns} \tag{C9}$$

with, according to (C7),

$$\tilde{\Pi}_0(k,n)=-\tilde{\rho}_0\int_0^1 ds\, e^{-(\lambda^2k^2/2)s(1-s)}e^{2i\pi ns} \tag{C10}$$

By introducing (C9) and (C4) and using the convolution theorem, the series (C4) can be summed with the result

$$\phi^{\text{eff}}(k,s)=\sum_{n=-\infty}^{\infty}\phi^{\text{eff}}(k,n)e^{-2i\pi ns}\ ,$$

with

$$\phi^{\text{eff}}(k,n)=\frac{U_0(k)}{1-U_0(k)\tilde{\Pi}_0(k,n)}\equiv\tilde{U}^{\text{eff}}_{\text{RPA}}(k,n)\ , \tag{C11}$$

where $\tilde{U}^{\text{eff}}_{\text{RPA}}(k,n)$ is the Boltzmann limit of $U^{\text{eff}}_{\text{RPA}}(k,n)$. The last identification in (C11) comes from (3.4). Finally, we obtain

$$\phi^{\text{eff}}(\mathbf{k},\xi_1,\xi_2)=\int_0^1 ds_1\int_0^1 ds_2 e^{-i\lambda\mathbf{k}\cdot[\xi_1(s_1)-\xi_2(s_2)]}\sum_{n=-\infty}^{\infty}e^{-i2\pi n(s_1-s_2)}\tilde{U}^{\text{eff}}_{\text{RPA}}(k,n)\ . \tag{C12}$$

The long-wavelength behavior of $\phi^{\text{eff}}(k,n)=\tilde{U}^{\text{eff}}_{\text{RPA}}(k,n)$ is easily investigated. In the regime where the Fermi statistics are suppressed $\lambda^2p^2/2\gg\beta\mu$ and, according to (3.3), $n_0(p)\to e^{\beta\mu}(e^{-(\lambda^2p^2/2)})$ while $1-n_0(p)\to1$. Then, according to (3.6), (3.8), and (A11),

$$\Gamma_1\to\frac{\tilde{\rho}_0}{2},\quad \Gamma_2\to-\frac{\tilde{\rho}_0}{2},\quad \text{and}\quad \Gamma_3\to\frac{\tilde{\rho}_0}{4}\ , \tag{C13}$$

and the limit of (3.5) is

$$\tilde{\Pi}_0(k,n)=-\tilde{\rho}_0\left[\delta_{n,0}(1-\tfrac{1}{12}\lambda^2k^2)+(1-\delta_{n,0})\frac{1}{4\pi^2n^2}\lambda^2k^2\right]+O(k^4)\ . \tag{C14}$$

[We note that (C14) can also be verified by expanding directly (C10) for small $\mathbf{k}$'s.] In the same way, by taking the Boltzmann limit (C13) in (3.9), we obtain

$$\lim_{k\to0}\phi^{\text{eff}}(k,n)\approx\delta_{n,0}\tilde{U}^{\,*}_{\text{DH}}(k)+(1-\delta_{n,0})U_0(k)\tilde{h}(n)\ , \tag{C15}$$

where $\tilde{U}^{\,*}_{\text{DH}}(k)$ is the Boltzmann limit of $U^{*}_{\text{DH}}(k)$. According to (3.11), (3.12), and (C13), $\tilde{U}^{\,*}_{\text{DH}}(k)$ is the Debye-Hückel potential associated with the density $\tilde{\rho}_0$ and the renormalized charge $\tilde{e}^{\,*}=e/\sqrt{1-(\tilde{\kappa}^{\,0}_D\lambda^2)/12}$,

$$\tilde{U}^{\,*}_{\text{DH}}(k)=\frac{4\pi\beta\tilde{e}^{\,*2}}{k^2+\tilde{\kappa}^{\,*2}_D}\ , \tag{C16}$$

with $\tilde{\kappa}^{\,*}_D=\sqrt{4\pi\beta\tilde{\rho}_0\tilde{e}^{\,*2}}$. Similarly, $\tilde{h}(n)$ is the Boltzmann

limit of $h(n)$ given by (3.10),

$$\tilde{h}(n)=\frac{1}{1+(\tilde{\kappa}_D^{02}\lambda^2/4\pi^2n^2)}\ , \tag{C17}$$

with $\tilde{\kappa}_D^0=\sqrt{4\pi\beta\tilde{\rho}_0e^2}$.

Therefore, one sees that only the zero-frequency component of the effective potential is screened. This suggests to split $\phi^{\text{eff}}(\mathbf{k},\xi_1,\xi_2)$ given by (C12) into two parts, singling out its zero-freqency term. This leads to the decomposition (4.11) with

$$\phi_S^{\text{eff}}(\mathbf{k},\xi_1,\xi_2)=\frac{4\pi\beta e^2}{k^2-4\pi\beta e^2\tilde{\Pi}_0(k,0)}\int_0^1 ds_1\int_0^1 ds_2 e^{-i\lambda\mathbf{k}\cdot[\xi_1(s_1)-\xi_2(s_2)]} \tag{C18}$$

and

$$\phi_L^{\text{eff}}(\mathbf{k},\xi_1,\xi_2)=\int_0^1 ds_1\int_0^1 ds_2(e^{-i\lambda\mathbf{k}\cdot[\xi_1(s_1)-\xi_2(s_2)]}-1)\sum_{\substack{n=-\infty\\ n\neq 0}}^{\infty} e^{-i2\pi n(s_1-s_2)}\phi^{\text{eff}}(k,n)\ . \tag{C19}$$

It is clear on (C18) that $\phi_S^{\text{eff}}(\mathbf{k},\xi_1,\xi_2)$ is an infinitely differentiable function of $\mathbf{k}$; therefore, $\phi_S^{\text{eff}}(\mathbf{x},\xi_1,\xi_2)$ decays faster than any inverse power of $|\mathbf{x}|$. To determine the long-range behavior of $\phi_L^{\text{eff}}(\mathbf{x},\xi_S,\xi_2)$, we examine the most singular contribution of (C19) as $k\to 0$. One obtains it by using (C15) and by expanding the factor $(e^{-i\lambda\mathbf{k}\cdot[\xi_1(s_1)-\xi_2(s_2)]}-1)$ in (C19) to second order in $\mathbf{k}$ (the first order does not contribute since $\int_0^1 ds\, e^{-2i\pi ns}=\delta_{n,0}$) with the result

$$\lim_{|\mathbf{k}|\to 0}\phi_L^{\text{eff}}(\mathbf{k},\xi_1,\xi_2)\approx\lambda^2 4\pi\beta e^2\int_0^1 ds_1\int_0^1 ds_2\frac{[\mathbf{k}\cdot\xi_1(s_1)][\mathbf{k}\cdot\xi_(s_2)]}{|\mathbf{k}|^2}\tilde{h}(s_1-s_2)\ , \tag{C20}$$

where

$$\tilde{h}(s)=\sum_{\substack{n=-\infty\\ n\neq 0}}^{\infty}\tilde{h}(n)e^{-2i\pi ns}\ .$$

This leads to the dipolar behavior (4.12).

One sees that the singular term (C20) occurs at the orders $\hbar^n, n\geq 2$, because of the λ^2 prefactor. Thus the classical limit of the effective potential, $\phi^{\text{eff}(0)}(\mathbf{k},\xi_1,\xi_2)$, is obtained by setting λ equal to 0 in $\phi_S^{\text{eff}}(\mathbf{k},\xi_1,\xi_2)$. According to (C18) and (C10), $\phi^{\text{eff}(0)}(\mathbf{k},\xi_1,\xi_2)$ coincides with the Debye-Hückel potential associated with the density $\tilde{\rho}_0$

$$\phi^{\text{eff}(0)}(\mathbf{k},\xi_1,\xi_2)=\frac{4\pi\beta e^2}{k^2+\tilde{\kappa}_D^{02}}\equiv\tilde{U}_{\text{DH}}(k)\ , \tag{C21}$$

with $\tilde{\kappa}_D^0\equiv\sqrt{4\pi\beta\tilde{\rho}_0e^2}$. The term linear in $\hbar$ is

$$\hbar\phi^{\text{eff}(1)}(\mathbf{k},\xi_1,\xi_2)=\tilde{U}_{\text{DH}}(k)(-i\lambda)\mathbf{k}\cdot\left[\int_0^1 ds[\xi_1(s)-\xi_2(s)]\right]\ . \tag{C22}$$

Finally, since $D(\xi)$ is Gaussian,

$$\int D(\xi)e^{i\lambda\mathbf{k}\cdot\xi(s)}=e^{-(\lambda^2k^2/2)|s||1-s|}=-\tilde{\Pi}_0(k,s)/\tilde{\rho}_0\ ,$$

according to (C7); then integrating (C19) on ξ_1 gives a factor

$$-[\tilde{\Pi}_0(k,s_1)/\tilde{\rho}_0]e^{i\lambda\mathbf{k}\cdot\xi_2(s_2)}-1\ .$$

Since

$$-[\tilde{\Pi}_0(k,s_1)/\tilde{\rho}_0]=1+O(k^2)$$

[see (C14)] and

$$\int_0^1 ds_1\sum_{\substack{n=-\infty\\ n\neq 0}}^{\infty} e^{-i2\pi ns_1}=0\ ,$$

integrating (C19) on ξ_1 kills the Coulombic singularity $1/k^2$ of $\phi^{\text{eff}}(k,n)$ for $n\neq 0$. We conclude that after integration on one of its ξ variables, the effective potential becomes short range.

*Present address: Laboratoire de Physique Théorique ENSLAPP, Ecole Normale Supérieure de Lyon, 46 allée d'Italie, F-69364 Lyon, France.

[1] A. Alastuey and Ph. A. Martin, Phys. Rev. A **40**, 6485 (1989).
[2] D. Brydges and P. Federbush, Commun. Math. Phys. **73**, 197 (1980).
[3] J. Imbrie, Commun. Math. Phys **87**, 515 (1983).
[4] A. Fetter and J. D. Walecka, *Quantum Theory of Many-Particle Systems* (McGraw-Hill, New York, 1971).
[5] D. Pines and Ph. Nozières, *The Theory of Quantum Liquids* (Benjamin, New York, 1966).
[6] Ph. A. Martin and Ch. Oguey, J. Phys. A **18**, 1995 (1985).
[7] J. Ginibre, J. Math. Phys. **6**, 238 (1965); **6**, 252 (1965); **6**, 1432 (1965).
[8] J. E. Mayer, J. Chem. Phys. **18**, 1426 (1950).
[9] R. Abe, Prog. Theor. Phys. **27**, 213 (1959).
[10] F. H. Stillinger and R. Lovett, J. Chem. Phys. **48**, 3858 (1968); **49**, 1991 (1968). We note that the classical sum rule (4.41) can be obtained from the quantum sum rule (2.17). Indeed, in the classical limit $\lambda\kappa_D$ vanishes so that only the term $n=0$ does contribute in (2.17).
[11] D. Pines, *The Many-Body Problem* (Benjamin, New York, 1961), Chap. 3.